Received: 1 April 2021 | Revised: 5 July 2021 | Accepted: 7 July 2021

DOI: 10.1002/jms.4777

RESEARCH ARTICLE

Journal of MASS SPECTROMETRY WILEY

Determination of trace compounds and artifacts in nitrogen background measurements by proton transfer reaction time-of-flight mass spectrometry under dry and humid conditions

Jorge Iván Salazar Gómez[1] | Martha Sojka[1] | Christian Klucken[1] | Robert Schlögl[1,2] | Holger Ruland[1]

[1]Department of Heterogeneous Reactions, Max Planck Institute for Chemical Energy Conversion, Mülheim a.d. Ruhr, Germany

[2]Department of Inorganic Chemistry, Fritz Haber Institute of the Max Planck Society, Berlin, Germany

Correspondence
Jorge Iván Salazar Gómez and Holger Ruland, Department of Heterogeneous Reactions, Max Planck Institute for Chemical Energy Conversion, Stiftstrasse 34-36, 45470 Mülheim a.d. Ruhr, Germany.
Email: jorge-ivan.salazar-gomez@cec.mpg.de; holger.ruland@cec.mpg.de

Funding information
Bundesministerium für Bildung und Forschung, Grant/Award Numbers: 03EK3037C, 03EK3546; Max Planck Society

Abstract

A qualitative analysis was applied for the determination of trace compounds at the parts per trillion in volume (ppt_v) level in the mass spectra of nitrogen of different qualities (5.0 and 6.0) under dry and humid conditions. This qualitative analysis enabled the classification and discovery of hundreds of new ions (e.g., $[S_x]H^+$ species) and artifacts such as parasitic ions and memory effects and their differentiation from real gas impurities. With this analysis, the humidity dependency of all kind of ions in the mass spectrum was determined. Apart from the inorganic artifacts previously discovered, many new organic ions were assigned as instrumental artifacts and new isobaric interferences could be elucidated. From 1140 peaks found in the mass range *m/z* 0–800, only 660 could be analyzed due to sufficient intensity, from which 463 corresponded to compounds. The number of peaks in nitrogen proton transfer reaction (PTR) spectra was similarly dominated by nonmetallic oxygenated organic compounds (23.5%) and hydrocarbons (24.1%) Regarding only gas impurities, hydrocarbons were the main compound class (50.2%). The highest contribution to the total ion signal for unfiltered nitrogen under dry and humid conditions was from nonmetallic oxygenated compounds. Under dry conditions, nitrogen-containing compounds exhibit the second highest contribution of 89% and 96% for nitrogen 5.0 and 6.0, respectively, whereas under humid conditions, hydrocarbons become the second dominant group with 69% and 86% for nitrogen 5.0 and 6.0, respectively. With the gathered information, a database can be built as a tool for the elucidation of instrumental and intrinsic gas matrix artifacts in PTR mass spectra and, especially in cases, where dilution with inert gases plays a significant role.

KEYWORDS
gas impurities, gas traces, industrial gases, proton transfer reaction time-of-flight mass spectrometry, volatile organic compounds

1 | INTRODUCTION

In many analytical procedures and catalytic reactions, the utilization of inert gases, such as nitrogen, helium, or argon, is unavoidable. Nitrogen is used in many applications, for example, purging gas in sampling methods,[1–3] carrier gas in diluting and gas generating systems,[4–9] in surface area measurements of porous materials,[10,11] as reactant in the Haber–Bosch process,[12] in cryogenic sampling applications,[13,14] and as carrier gas in gas chromatography (GC).[15–17] Because in all of these applications the gas quality used is usually 5.0 (99.999% purity) or 6.0 (99.9999% purity), the remaining volatile organic compounds (VOCs) and water do not pose an interference to the different applications. However, in the analysis of traces at the parts per trillion in volume (ppt_v) level, ultrapure gases are required. One technique that offers on-line measurements with high sensitivity at the ppt_v level is proton transfer reaction mass spectrometry (PTR-MS).[18] This technique is a powerful tool for the on-line monitoring of trace amounts of VOCs without requiring additional preseparation techniques such as GC. PTR-MS was developed to determine VOCs in air and has found application in a variety of fields such as breath analysis,[19,20] environmental science,[18,21–23] life[18,20] and food science,[24–26] process monitoring,[27–30] and studies on industrial or catalytic applications.[31–40] The main advantage of PTR-MS is its soft ionization of molecules by the primary ion H_3O^+, which implies that the ion-molecule process during the PTR is almost nondissociative. This low fragmentation can be used for the detection of molecules at their molecular mass plus one H^+, and thus, it enables the analysis of complex gas mixtures without the need for previous separation methods. One of the drawbacks of this technique is that isomeric compounds cannot be distinguished. Additionally, only if the mass resolution of the instrument is above 4000 $m/\Delta m$, some isobaric compounds can be identified.[41] However, the coupling of a time-of-flight mass analyzer to a PTR ion source and a drift tube (PTR-TOF-MS) brought a remarkable enhancement of the sensitivity.[42] The advantages of TOF over quadrupole mass filters are their higher mass resolution, their short response time (1 s or less), the simultaneous measurement of the whole mass spectrum, and a virtually unlimited mass range. However, PTR-TOF-MS spectra are very complex, and for gas matrices with a high number of VOCs, their interpretation becomes very challenging. Therefore, an effective method for the elucidation of instrument artifacts was developed,[43] and the artifacts were found to be mainly nitrogen-containing or metallic ions.

The dynamic of the background and its humidity dependency is of crucial interest in order to distinguish possible memory effects and organic artifacts, for example, for the validation of feed gas purification in carbon capture and usage (CCU) applications exemplified by the Carbon2Chem® project.[44,45] This project aims to utilize the process gases of a steel mill plant, coke oven gas, blast furnace gas, and basic oxygen furnace gas, for the production of chemicals like methanol or ammonia. A detailed analysis of the three steel mill gases is required, especially with respect to the trace compounds in these gases, to determine the necessary gas purification for their application and to prove the efficacy of the chosen gas purification to ensure a long lifetime of the catalysts applied in subsequent processes.

According to Equation 1, the main condition for the proton transfer to occur is that the analyte gases must possess a proton affinity (PA) higher than water (691 kJ mol^{-1}):

$$R + H_3O^+ \rightarrow [R]H^+ + H_2O, \quad (1)$$

where R is a gas-phase analyte. This reaction is exothermic and proceeds at reaction rates, which are close to the rate of collision (approximately: 10^{-9} cm^3 $molecule^{-1}$ s^{-1}). An advantage of PTR-TOF-MS is that the main components of air, such as nitrogen, oxygen, carbon dioxide, and methane, exhibit lower proton affinities than water and, therefore, are not measurable under standard conditions. This enables the characterization of VOCs in air and many other gas matrices without the need of dilution, which enhances the detection limit for VOCs. The main drawback of PTR is the presence of parasitic ions, such as NO^+, O_2^+, water clusters $[(H_2O)_n]H_3O^+$, $[NH_3]H^+$, and $[N_2]H^+$. The presence of small amounts of NO^+ and O_2^+ has been ascribed to back diffusion of air from the drift tube region.[46] These ions should not account for more than 2% of the primary ion signal to avoid unwanted side reactions.[47,48] In theory, that is, in the absence of back diffusion, only water molecules are present in the ion source, and after electron impact, the H^+, O^+, H_2^+, OH^+, and H_2O^+ ions are formed. Subsequently, these ions can react with further water molecules in the "source drift region" and produce H_3O^+ ions with a purity of about 99.5%.[19]

In contrast to the usual environmental applications of PTR-MS,[49,50] in which humidity and gas matrix composition does not fluctuate significantly, in catalytic processes, the gas composition can change from dry to a humid regime (e.g., methanol synthesis). Additionally, in most applications, the gas samples do not need to be diluted with some inert gas, because the concentration of the analytes is already in the desired parts per million in volume (ppb_v) range. Sometimes, even sample preconcentration is necessary[51] in order to increase the sensitivity of the method.[52] However, for the characterization of VOCs in industrial gases, dilution becomes necessary to avoid pressure changes in the detection region of the instrument and to prevent saturation of the detector, thus remain in the linearity range of the detector.[31] To avoid detector saturation in the analysis of industrial gases without losing too much sensitivity is challenging, because the concentration range of many compounds of interest may be quite different and often exhibit significant temporal fluctuations. This could mean that the concentration of certain analytes, which exhibit concentrations in the ppb_v range can fall below the detection limit of the instrument after dilution, making their identification and quantification challenging. Simultaneously, other compounds could exhibit concentration peaks, which compromise the required measurement criterion $[H_3O^+] \geq 10^6$ counts per second (cps),[21] making dilution mandatory to obtain reliable results.

Contrary to GC, where the oven and some gas lines can be heated up to high temperatures to bake out the columns to degas residuals in the system, in PTR-TOF-MS, this procedure is limited by

the relative low operating temperatures (<120°C), and therefore, a knowledge of the contribution of memory effects on the background becomes important. Furthermore, if dilution is required, the contribution of VOCs in the diluting gas like N_2 to the background has to be known. It has been shown that, sometimes, background levels can be quite high[51] and that background signals for many ions are dependent on humidity.[50] To our knowledge, apart from our previous study on artifacts in PTR instruments,[43] there has not been any study regarding impurities and artifacts in nitrogen of different qualities. In this work, qualitative analysis of background measurements using nitrogen 5.0 (99.999% purity) and nitrogen 6.0 (99.9999%) in a proton transfer reaction quadrupole interface time-of-flight mass spectrometer (PTR-QiTOF)[53] were carried out to distinguish between instrumental artifacts (instrumental background[54]), memory effects (setup background[54]), and real gas impurities (chemical background[54]). In order to reveal impurities in these gases, which may also be present as memory effects, a comparison was carried out under dry and humid conditions, and for N_2 6.0, also, a further purification by a filter was implemented. For the characterization of trace compounds in complex gas matrices, such as industrial off-gases or the products of some catalytic reactions, it is crucial to understand the contribution of artifacts to the mass spectrum. These artifacts may originate from the instrument (e.g., parasitic ions or memory effects), gas lines (e.g., memory effects), or carrier gas (e.g., impurities and their possible fragments) and can coincide with some substances of interest or can even cause side reactions. The gathered information in this study will serve to build up a spectral database, which can be applied later on to simplify the analysis of complex spectra obtained by PTR-MS.

2 | MATERIALS AND METHODS

2.1 | Gas samples and setup

The experiments with the PTR-QiTOF at the steel mill plant of ThyssenKrupp Steel Europe in Duisburg, Germany, before the relocation of the lab container[35] to the Carbon2Chem technical center[55] were carried out with N_2 5.0 (99.999% purity) and N_2 6.0 (99.9999% purity) purchased from Linde Gas, Duisburg, Germany. Prior to the measurements, the setup comprising the calibration gas generator, the transfer line, the multiport valve (MPV), and the PTR-QiTOF were heated up to the desired temperatures and simultaneously purged for about 30 min with the respective nitrogen gas quality. After every experiment, the system was continuously purged for additionally 25 min. Nitrogen 6.0 was analyzed first for about 30 min and subsequently nitrogen 5.0. In every experiment, the first 10 min were measured under dry conditions, and subsequently for 15 min, the humidity was set to 50% relative humidity (RH). Because the filter line was separate, this measurement was carried out with nitrogen 6.0 after the nitrogen 5.0 experiment. After the relocation of the lab container, the validation experiments with the nickel and charcoal filters shown in the Supporting Information were carried out for about 20 h using nitrogen 6.0 purchased from AIR LIQUIDE Deutschland GmbH, Oberhausen, Germany. The raw gas measurement was carried out for about 30 min. All the measured gases were connected to a Sulfinert®-coated flow-through 10-MPV from VICI Valco. The dry and humidified gases for the background measurements were generated using a certified calibration gas generator (HovaCal)[56] from IAS GmbH, Oberursel, Germany, which can generate gas standards of typical VOCs from a few ppb up to higher ppm level under dry or humid conditions. All components such as evaporators and gas lines were coated with Sulfinert®. The humidification of the gases was carried out using Milli-Q® water stored in DURAN® glass bottles used as reservoirs connected to the calibration gas generator. For the nitrogen 6.0, which was additionally purified with a filter, no humidification was possible, because the measurements with this extra-purified gas were carried out in a separate line, in order to identify possible artifacts coming from the calibration gas generator and from the filter themselves. The validation experiment with the HPLC-grade water from Sigma-Aldrich shown in the Supporting Information was carried out for 2 h and 20 min. The reactive filters used contained nickel and nickel monoxide as the main constituents and were purchased from the company Rainer Lammertz Pure Gas Products, Huerth, Germany. The charcoal filter used for validation was purchased from Supelco®. The heated line (150°C) connecting the calibration gas generator to the MPV had also a Sulfinert® coating. Comparison experiments were carried out with an uncoated stainless steel transfer line and a polytetrafluoroethylene (PTFE) hose.

2.2 | Proton transfer reaction time-of-flight mass spectrometry

A detailed description of the type of PTR-QiTOF instrument used in this study has been given by Sulzer et al.[53] In brief, the PTR-QiTOF was located in a lab container on a steel mill plant in the Ruhr area in Germany. The instrument was acquired from Ionicon Analytik GmbH, Innsbruck, Austria. In this study, measurements were conducted using H_3O^+ as primary ion. H_3O^+ ions were generated in the hollow cathode ion source using a water vapor flow of 7 sccm. The drift tube parameters were set to 900 V, 3.50 mbar, and 60°C resulting in a reduced electric field (E/N) of 131 Td. An E/N range between 120 and 140 Td has been established as a standard value, because it is a good compromise between excessive water cluster formation and product ion fragmentation.[20,46] The inlet lines of PTR-QiTOF were made of polyether ether ketone (PEEK). The inlet temperature was set to 100°C. No additional inlet flow was set (0.0 ml min^{-1}). The default flow of the PTR-QiTOF was ~106 ml min^{-1}. In the detection region, orthogonal acceleration in the V-mode was used. A mass range from *m/z* 15 up to 797 was chosen for the nontarget screening measurements. The cycle time was set to 1 s. The spectra were acquired at a frequency of 20 kHz. Every spectrum is the sum of 20,000 acquisitions lasting for about 2 μs each. The collected signals were corrected for the instrumental transmission and normalized to the primary ion. Mass calibration was carried out using the masses of the internal

standard equipped in the PTR-QiTOF, the so-called PerMaSCal® (1,3-diiodobenzene) at *m/z* 203.943 ($C_6H_5I^+$) and at *m/z* 330.848 ($[C_6H_4I_2]H^+$) as well as the masses of NO^+ (*m/z* 29.997) and the second isotope of H_3O^+ ($H_3{}^{18}O^+$, *m/z* 21.022). For simplicity, in the following, it is referred to the second, third, and so on isotopes by using a nomenclature according to their order of abundance, for example, $H_3{}^{16}O^+$ ($H_3O^+(1)$ or simply H_3O^+), $H_3{}^{18}O^+$ ($H_3O^+(2)$), and so on. Prior to measurements, an optimization was carried out with the Thuner Software (TofWerk, Thun, Switzerland). Optimization of the masses of the parasitic ions $[N_2]H^+$ (*m/z* 29.013), NO^+ (*m/z* 29.997), and $O_2{}^+$ (*m/z* 31.989) was conducted in order to minimize their intensities. The masses of protonated toluene (*m/z* 93.070) and the two known masses from the internal standard PerMaSCal® were set in order to maximize their sensitivities.

3 | RESULTS AND DISCUSSION

The ion distributions of the primary ion and the water clusters in the PTR-QiTOF using nitrogen 5.0 under dry and humid conditions (50% RH at 20°C) have been previously shown.[43] The relative abundance of the water cluster in the dry gas is only 0.13%. However, under humid conditions, a contribution of approximately 13% is observed, which is in accordance to the values reported by Pang.[46] Nitrogen 6.0 exhibits a similar ion distribution.[43] In brief, the applied method to differentiate instrument artifacts (instrumental background[54]), memory effects (setup background[54]), and gas impurities (chemical background[54]) consists in comparing the signals of the ions in N_2 5.0 and N_2 6.0 under dry and humid conditions to determine instrument artifacts, because these are independent of the gas quality, and after an additional purification of the purer N_2 6.0 with a filter, the gas impurities and memory effects can be distinguished. For all comparative spectra of N_2 6.0 after filtering with a high-purity filter, it is assumed that the filter works efficiently in the removal of VOCs and due to the expected low concentrations of VOCs in such pure gases, the loading capacity of the filter is not reached. If for a gas impurity after filtering still some signal remains, the remaining signal at this concentration level is then assigned as a combination of memory effects in the pipelines, the PTR-QiTOF, and breakthrough of VOCs through the filter. For most VOCs, the specifications from the manufacturer of the reactive filter are <1 ppt_v, and therefore, the main contribution is attributed to memory effects. Because the concentrations of VOCs in nitrogen 5.0 and 6.0 are very low, in most cases, the contributions of the second and third isotopologues of a compound were in the instrumental noise level and, therefore, were not considered. An intensity of at least 3σ higher than the average noise level was considered as criterion applied for the peak assignment, where sigma is the standard deviation of the mean values obtained from the number of cycles measured. Because a complete description of all ions found up to *m/z* 800 is not possible, only selected ions are being discussed here. A complete list of all ions with their assignments as artifact, memory effect, or gas impurity and their humidity dependencies are given in Tables S1 and S2, respectively.

3.1 | Setup artifacts

Because the measurements were carried out in a mobile container[35] designed for the on-line characterization of trace compounds in metallurgical gases directly on site, it was of interest to elucidate possible artifacts originated from the whole setup. The setup for the nitrogen background measurements comprised the calibration gas generator, the MPV and Sulfinert® gas lines, the PTR-QiTOF, and a separate gas line for the filtered N_2 6.0. The artifacts, which originate from the instrument itself (ion source, drift tube or quadrupole interface), are mostly reported elsewhere in detail.[43] Regarding the calibration gas generator HovaCal, only two artifacts were identified: the $[H_3BO_3]H^+$ ion at *m/z* 63.025 and the $[H_3BO_3]H_3O^+$ association ion at *m/z* 81.035. These artifacts were mainly measurable under humid conditions, when the pure Milli-Q® water was injected into the vaporizers of the HovaCal for humidification. A detailed description is given in Sections 3.3 and 3.4, respectively. Analogous to the boron compounds, three silicon-containing ions were observed: the $(CH_3)_2OHSi^+$ ion at *m/z* 75.026, the $(OH)_3Si^+$ ion at *m/z* 78.985, and the $[(CH_3)_2(OH)_2Si]H^+$ ion at *m/z* 93.037. These ions are presumed to originate from the Sulfinert® coating mainly under humid conditions and showed no correlation to higher siloxanes also found in the background measurements. A detailed description is given in Sections 3.3 and 3.4, respectively.

3.1.1 | From filter

In the analysis of the background of nitrogen, it was important to verify if the filter used for further purification of N_2 6.0 produces any kind of artifacts. The comparison of the spectra in Figure 1 showed that the sulfur species $[S_4]H^+$ (*m/z* 128.896), $[S_6]H^+$ (*m/z* 192.840), $[S_8]H^+$ (*m/z* 256.789), and $[C_9H_8O]H^+$ (*m/z* 133.065) are only visible in the filtered N_2. To our knowledge, these sulfur species have not been in PTR-MS studies before. The latter have been previously reported[57,58] and ascribed as methylbenzofuran. It remains unclear why this compound seems to originate from the filter. In the unfiltered dry N_2 6.0, a signal of about 83% smaller is observed, which indicates that this compound is not a contaminant in N_2 6.0 but it can rather be associated to a remaining memory effect in the PTR-QiTOF. Especially, the detection of sulfur species as potent poisons is of paramount interest for catalytic applications. For the case of the determined sulfur species S_4, S_6, and S_8, their formation is thought to occur after the accumulation of different sulfur-containing VOCs (e.g., H_2S, thiols, COS and CS_2) still present in N_2 6.0 on active centers at the surface of the nickel/nickel oxide filter. They may also originate from the filter itself, as S_x is a genuine trace impurity of all nickel metal samples[59–62] where it can segregate from the bulk, especially when exposed to oxygen-[63] or hydrogen-containing gases. A further discussion on the sulfur species and their origin can be found in the Supporting Information.

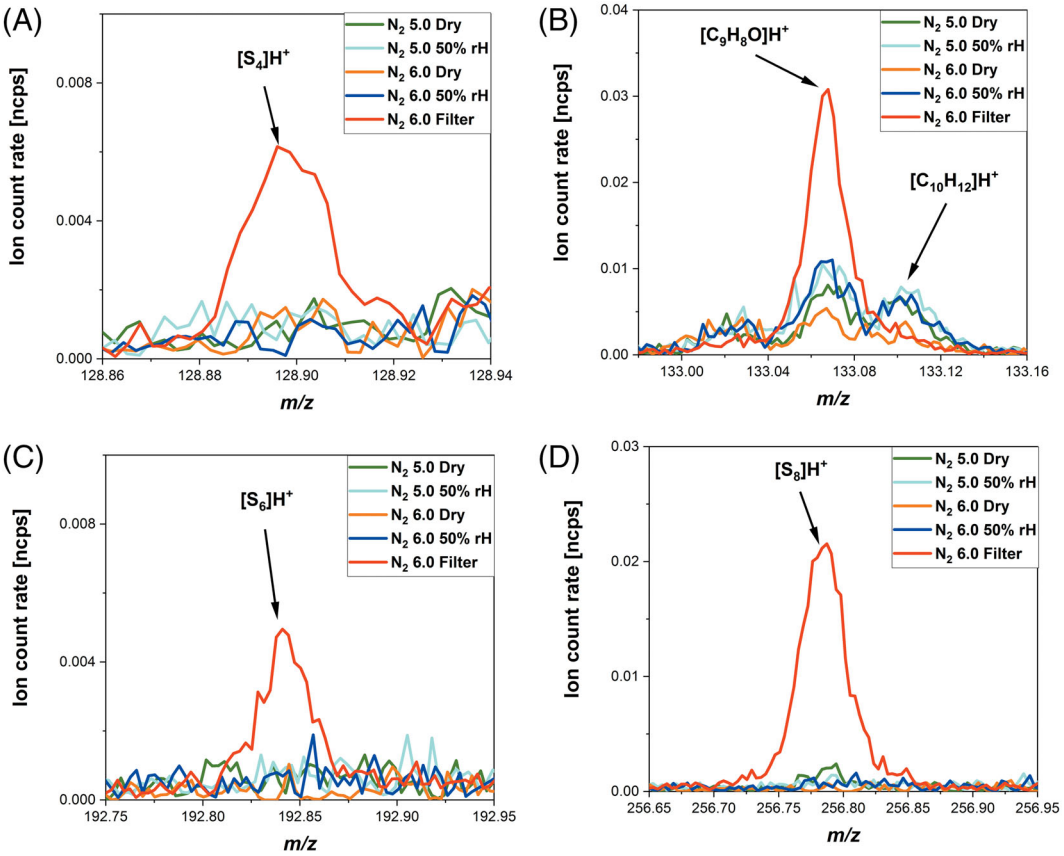

FIGURE 1 Comparison of the profile mass spectra of species arising in the filtering process (A) $[S_4]H^+$, (B) $[C_9H_8O]H^+$, (C) $[S_6]H^+$, and (D) $[S_8]H^+$, measured in nitrogen background under dry and humid conditions (50% relative humidity [RH] at 20°C) using H_3O^+ as primary ion in a proton transfer reaction quadrupole interface time-of-flight mass spectrometer (PTR-QiTOF) at a reduced electric field (E/N) of 131 Td

3.1.2 | Internal standard PerMaSCal®

Contributions to the spectrum from the internal standard PerMaSCal® (1,3-diiodobenzene, $C_6H_4I_2$) were of interest in order to avoid misinterpretations, because in the envisaged nontarget analysis of the three metallurgical gases, the whole spectrum needs to be considered. Normally, most PTR studies focus on small mass ranges or single compounds, and therefore, a detailed spectrum of the internal standard is not relevant as it is only used for the mass calibration. However, for nontarget studies, a knowledge of all contributions to the spectrum is required. It is known that the 1,3-diiodobenzene protonates to give the $[C_6H_4I_2]H^+$ ion at *m/z* 330.848 (Figure 2D) and fragments to give the $C_6H_5I^+$ ion at *m/z* 203.943 (Figure 2A). The latter ion is rather unexpected because the loss of an iodine atom would lead to the $C_6H_4I^+$ ion, which is energetically unfavorable. Therefore, a concerted reaction with water may take place, but the mechanism remains unclear. Under dry conditions, due to the higher collision energy, more fragmentation is expected. At *m/z* 219.962 (Figure 2B), a reaction channel to $[C_6H_4INH_2]H^+$ is observed, possibly through a nucleophilic substitution with ammonia. This is plausible because ammonia is an artifact produced in the ion source of the PTR-QiTOF.[43] In Figure 2C, a similar reaction channel at *m/z* 220.946 is observed to form $[C_6H_4IOH]H^+$ but with water as reagent. Additional reaction channels after the substitution of a H atom were also observed at *m/z* 345.858 ($[C_6H_3I_2NH_2]H^+$) and *m/z* 346.842 ($[C_6H_3I_2OH]H^+$), whereas the $[C_6H_4I_2]H_3O^+$ ion was not observed even under humid conditions.

3.2 | Mass range *m/z* 40–60

In the mass range below *m/z* 40, there are only a few contributions to the mass spectrum, which have been described previously.[43] Worth mentioning is $[HCN]H^+$, which appears as an artifact and exhibits a negative humidity dependency of about 63%. In the specific case of HCN, which is similar to that of formaldehyde, its PA is just slightly higher (PA = 712.9 kJ mol^{-1}) than that of water (PA = 691 kJ mol^{-1}), and therefore, the backward reaction plays a role at high humidities.[64] In the mass range *m/z* 40–60, predominantly hydrocarbons and O-containing species were found as impurities in N_2. Figure 3A shows a peak at *m/z* 41.039, which is normally reported as $C_3H_5^+$ and is associated with fragments of a variety of compounds (e.g., 1-butene, propyne, and C4–C9 saturated and unsaturated alcohols)[65] and many hydrocarbons.[66] However, this ion has also been ascribed as a fragment of propene after losing H_2.[34] Such dehydrogenation processes

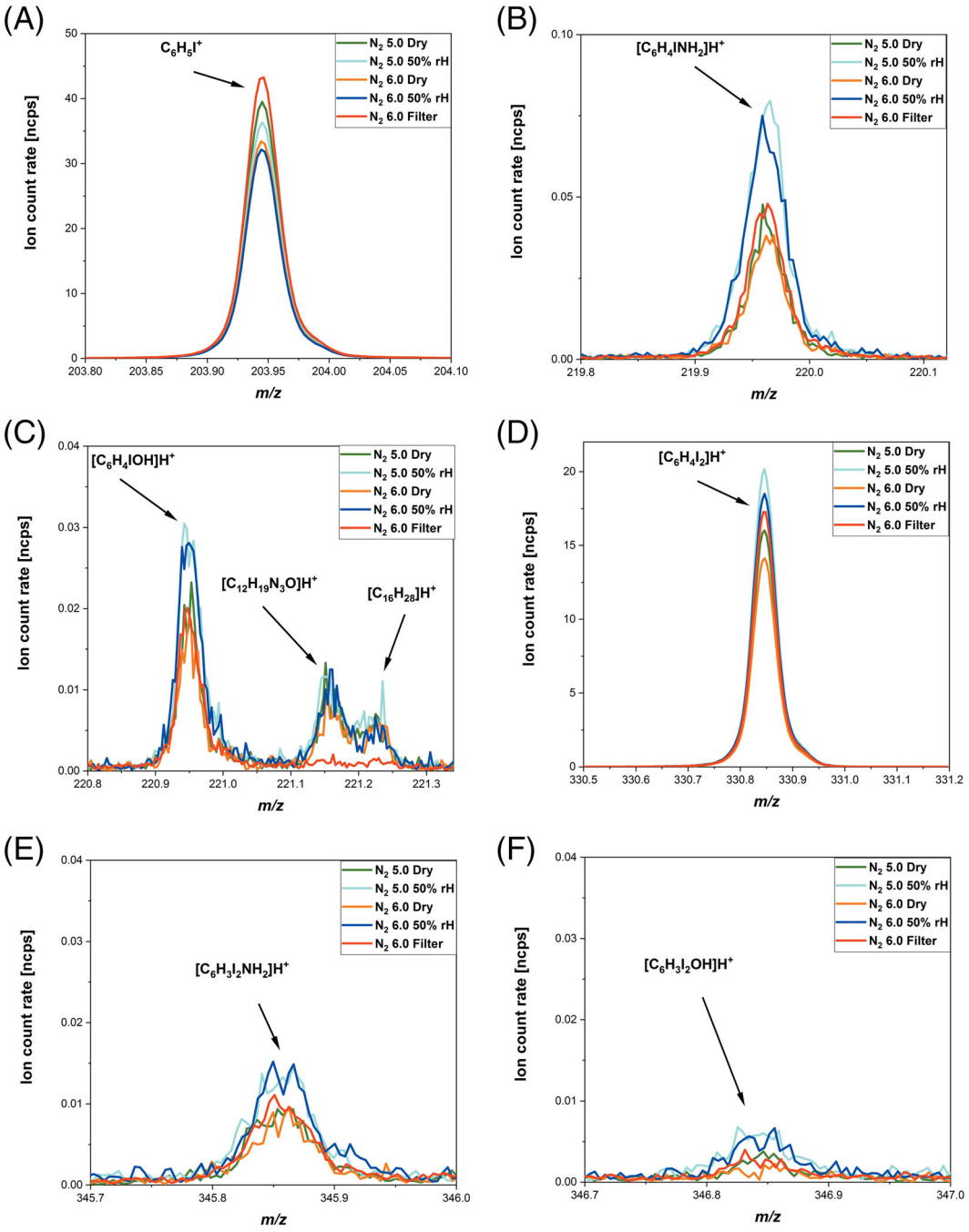

FIGURE 2 Comparison of the profile mass spectra of the main ions of the internal standard PerMaSCal and some byproducts (A) $C_6H_5I^+$, (B) $[C_6H_4INH_2]H^+$, (C) $[C_6H_4IOH]H^+$, (D) $[C_6H_4I_2]H^+$, (E) $[C_6H_3I_2NH_2]H^+$, and (F) $[C_6H_3I_2OH]H^+$, measured in nitrogen background under dry and humid conditions (50% relative humidity [RH] at 20°C) using H_3O^+ as primary ion in a proton transfer reaction quadrupole interface time-of-flight mass spectrometer (PTR-QiTOF) at a reduced electric field (E/N) of 131 Td

in PTR measurements, especially under dry conditions, have been previously observed.[67] Based on our elucidation method,[43] the peak at *m/z* 41.039 is assigned as gas impurity, which can be associated to 1,2-propadiene, because after filtering, a signal reduction of about 55% is observed for N_2 6.0, but the remaining signal still indicates some grade of memory effect or the contribution of fragments from larger molecules. Although a fragment would also show a similar trend as its parent ion after filtering, higher signals would be expected under dry conditions due to more fragmentation. Under humid conditions (50% RH at 20°C), a signal increase of 4.2 and 9.8 times is observed for N_2 5.0 and N_2 6.0, respectively. This discrepancy can be assigned to the different contribution of fragments to this mass in N_2 5.0 and N_2 6.0. Propene (Figure 3B) shows after filtering with a signal decrease of 39% a similar trend to *m/z* 41, which may suggest that *m/z* 41 is not the fragment $C_3H_5^+$ but rather the protonated C_3H_4 product after the loss of a H_2 molecule from propene. Two isobaric

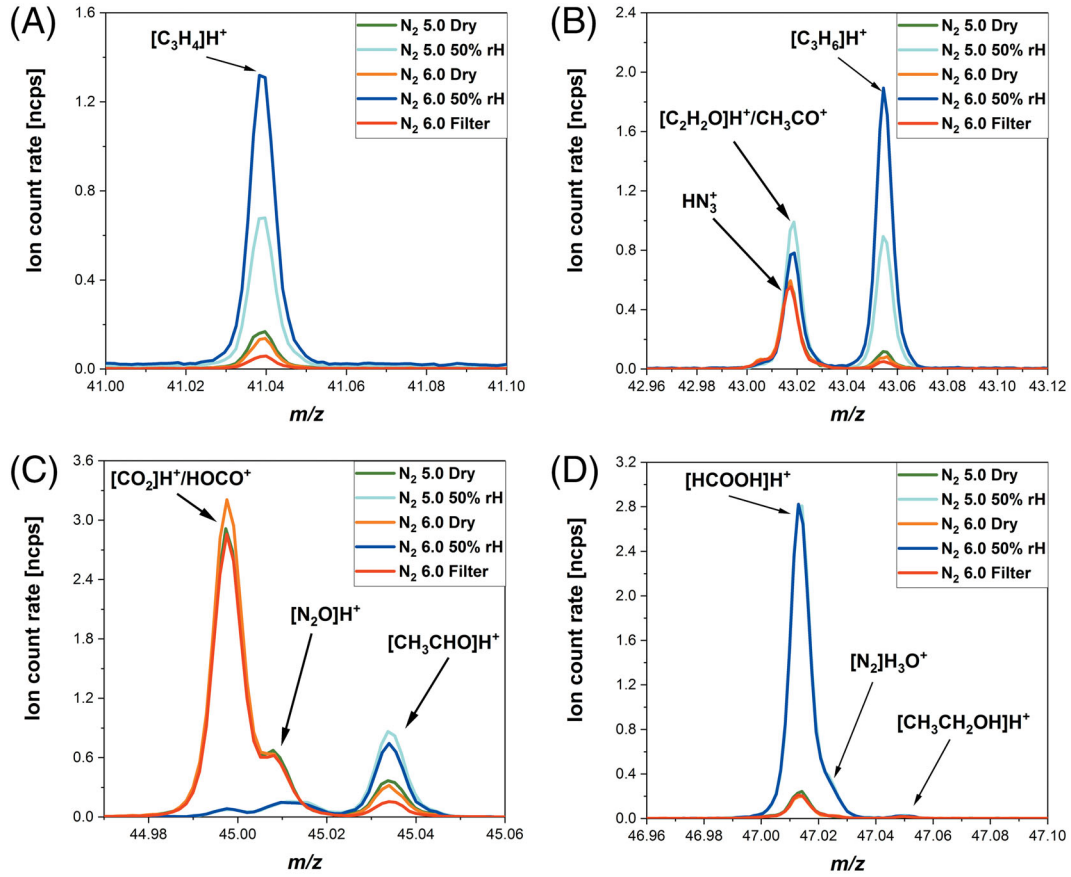

FIGURE 3 Comparison of the profile mass spectra of selected ions (A) $[C_2H_4]H^+$, (B) $[C_3H_6]H^+$, (C) $HCOO^+$, and (D) $[HCOOH]H^+$, measured in nitrogen background under dry and humid conditions (50% relative humidity [RH] at 20°C) using H_3O^+ as primary ion in a proton transfer reaction quadrupole interface time-of-flight mass spectrometer (PTR-QiTOF) at a reduced electric field (E/N) of 131 Td

artifacts can also be distinguished at *m/z* 43. The first one, HN_3^+, exhibits no humidity dependency, whereas CH_3CO^+, which has been previously reported as a fragment of oxygenated molecules,[49,51,68,69] exhibits a positive humidity dependency with a signal increase of 87% and 49% in N_2 5.0 and N_2 6.0, respectively.

By comparing Figure 3C,D, a close correlation between protonated formic acid ($[HCOOH]H^+$) and the fragment $HOCO^+$ (or HCO_2^+) can be established. It has been shown that the HCO_2^+ ion is not favorable because its energy level is about 400 kJ mol^{-1} higher than the $HOCO^+$ ($COOH^+$) ion.[70,71] Because the H—C bond is weaker than the H—O bond, fragmentation takes place at the H—C bond under dry conditions. Formic acid appears as instrument artifact showing a positive humidity dependency with a factor of about 12 times, whereas the opposite case occurs for the $HOCO^+$ ion with a signal increase of about 28 times under dry conditions, indicating more fragmentation. Although CO_2 is not expected to protonate due to its lower PA than water, it has been shown to give some signal after the extraction from the drift tube.[34] In ultrapure nitrogen (6.0) and after additional filtering, CO_2 is not expected, and therefore, the signal observed can exclusively be assigned to the $HOCO^+$ ion. In our case, we assign this ion as fragment of a carboxylic acid appearing as instrument artifact. In selected-ion flow-tube (SIFT) studies,[72] formic acid was shown to give only the protonated molecule as reaction channel. In contrast, in PTR-MS studies, the sensitivity of formic acid showed a negative humidity dependency.[68] Our finding is somehow surprising, because under humid conditions, a loss of OH after protonation would be expected, similar to alcohols. However, negative humidity dependencies for oxygenated compounds have been previously reported.[73] Besides the instrument artifacts, acetaldehyde appears as a VOC with a signal reduction of 48% after filtering and a positive humidity dependency of about 2.3 and 2.4 times for N_2 5.0 and N_2 6.0, respectively (Figure 3C).

Figure 4A shows a peak at *m/z* 55.054 assigned to the $[C_4H_6]H^+$ ion (most likely 1,3-butadiene), which appears as gas impurity and memory effect. It shows a signal reduction of 75% after filtering and can only be measured under dry conditions due to the overlapping with the water cluster $[(H_2O)_2]H_3O^+$. At *m/z* 57 (Figure 4B), four isobars can be recognized: CH_3NCO^+, $[C_3H_4O]H^+$,[74] $[(H_2O)_2]H_3O^+$(2), and $[C_4H_8]H^+$. The CH_3NCO^+ ion at *m/z* 57.021 appears as instrument artifact with a negative humidity dependency, which indicates it is the fragment of some large molecule. It derives highly probably after the loss of a H_2 from acetamide ($[CH_3CONH_2]H^+$, *m/z*

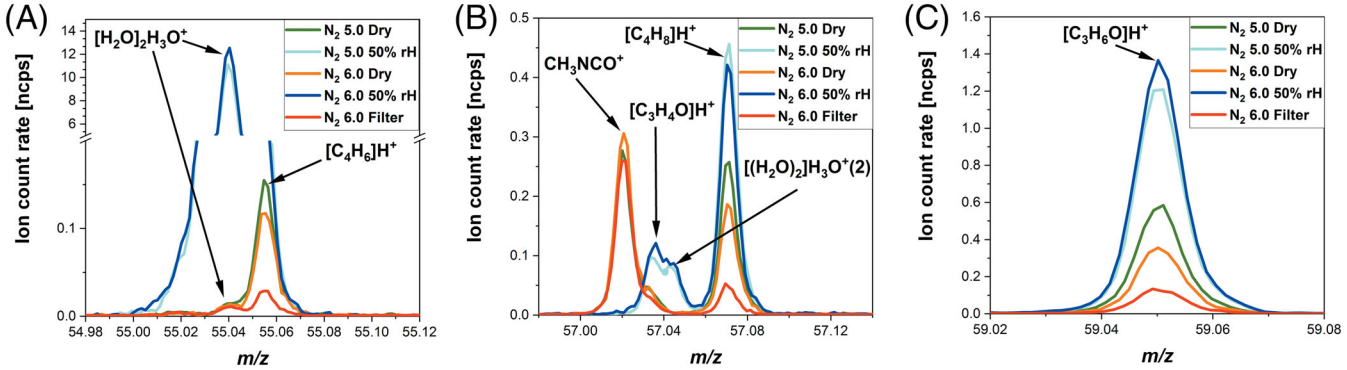

FIGURE 4 Comparison of the profile mass spectra of selected ions (A) $[C_4H_6]H^+$, (B) $[C_4H_8]H^+$, and (C) $[C_3H_6O]H^+$, measured in nitrogen background under dry and humid conditions (50% relative humidity [RH] at 20°C) using H_3O^+ as primary ion in a proton transfer reaction quadrupole interface time-of-flight mass spectrometer (PTR-QiTOF) at an reduced electric field (E/N) of 131 Td

60.044), which was first measured with PTR-TOF-MS in environmental samples.[75] In general, the H—N bond tends to be weaker than the H—C and H—O bonds, although the chemical environment plays a significant role.[76] An experimental value of 451 kJ mol^{-1} reported for the H—N bond in acetamide lies higher than typical values.[77] The $[C_3H_4O]H^+$ ion at *m/z* 57.034, associated to acrolein, becomes more visible under humid conditions (50% RH at 20°C) with a factor of about 3.7 times but interferes with the second isotope of the water cluster $[(H_2O)_2]H_3O^+(2)$ at *m/z* 57.043. For polar compounds, this positive humidity dependency is expected and can be associated with less fragmentation.[46] The higher sensitivity under humid conditions has been ascribed to the increased fraction of the water cluster ions in the drift tube of the PTR-MS with respect to the primary ion signal,[78] which at high abundancies lowers the average mobility of the reagent ions causing longer reaction times and less energetic collisions, resulting in a sensitivity increase.[78,79] Additionally, ligand switching reactions were proposed as a more general mechanism for causing a humidity-dependent sensitivity.[23] In SIFT studies, the peak at *m/z* 57.034 was assigned as a fragment ($C_2H_5CO^+$) of propanoic acid, a reaction channel with an exothermicity of 37.5 kJ mol^{-1}, and a contribution of 10%.[72]

The $[C_4H_8]H^+$ ion at *m/z* 57.070 (Figure 4B) has been reported as the fragment $C_4H_9^+$.[47] It is assigned here as gas impurity and memory effect, associated to *trans*-1,3-butadiene with a signal reduction of about 73% after filtering. Figure 4C shows a peak at *m/z* 59.049 normally associated with acetone,[80] which can also be assigned as gas impurity and memory effect with a signal reduction after filtering of about 62%. A proportionality between the signals of N_2 5.0 dry and N_2 5.0 50% RH as well as N_2 6.0 dry and N_2 6.0 50% RH was expected, showing a signal increase of about two and four times, respectively. However, it remains unclear why the signal of N_2 5.0 50% RH is not higher than the N_2 6.0 50% RH. This kind of positive humidity dependencies on sensitivity has been previously observed.[50,81] Hydrated product ions in the form of $[M]H_3O^+$ (where M is any VOC species) were not observed for acetone, in contrast to formic acid and ethanol (see Table S1).

3.3 | Mass range *m/z* 60–80

Acetic acid (Figure 5A) at *m/z* 61.028 was assigned as gas impurity and memory effect showing a signal drop between N_2 5.0 and N_2 6.0 of 36.4%. After filtering, an unexpected signal increase of 22% was observed, presumably due to the fragmentation of higher molecules caused by the dryer conditions. It exhibits a positive humidity dependency with a significant signal increase of about 8.3 and 10.4 times for N_2 5.0 and N_2 6.0, respectively. Apart from the expected sensitivity increase under humid conditions, an additional contribution to the signal due to surface stripping is plausible.[23] Acetic acid has been shown to exhibit strong memory effects, which results in high background levels, thus lowering the method sensitivity.[49] This compound has been previously measured in various environments.[23,57,68,69] The isobaric $[C_3H_8O]H^+$ ion at *m/z* 61.065 (Figure 5A) assigned to propanol is hardly measurable under both regimes, so if present, it may fragment completely to $C_3H_7^+$ (*m/z* 43.054). At *m/z* 63 (Figure 5B), two isobars are found. The first one can be assigned as artifact, corresponding most likely to the $CH_3O_3^+$ fragment (*m/z* 63.008), which does not show any humidity dependency. Another plausible ion, the $[CO_2]H_3O^+$ association ion, can be discarded due to the lack of humidity dependency. The second peak at *m/z* 63.026 was assigned to the formulas $[H_3BO_3]H^+$ or $[HBO_2]H_3O^+$ (*m/z* 63.025), which appears as a setup artifact originating from the Milli-Q® water or DURAN® glass bottles used for the humidification of the gas with the calibration gas generator. Under dry conditions, this ion exhibits a very low signal with a significant signal increase of a factor of about 156 times under humid conditions. A peak at *m/z* 63 has been previously reported as $NaBH_3CN^+$ (*m/z* 63.025), a reagent used in the synthesis of psychoactive substances.[82] This compound has also been found in the background of empty sample vials[83] but exhibited lower intensities under humid conditions, explained as due to the lower surface area available when the vial is filled with water. In our case, we rule out the $NaBH_3CN^+$ ion because the third most abundant isotope does not fit to the expected isotopic distribution and it is not a plausible contaminant in pure nitrogen. Protonated dimethyl sulfide or

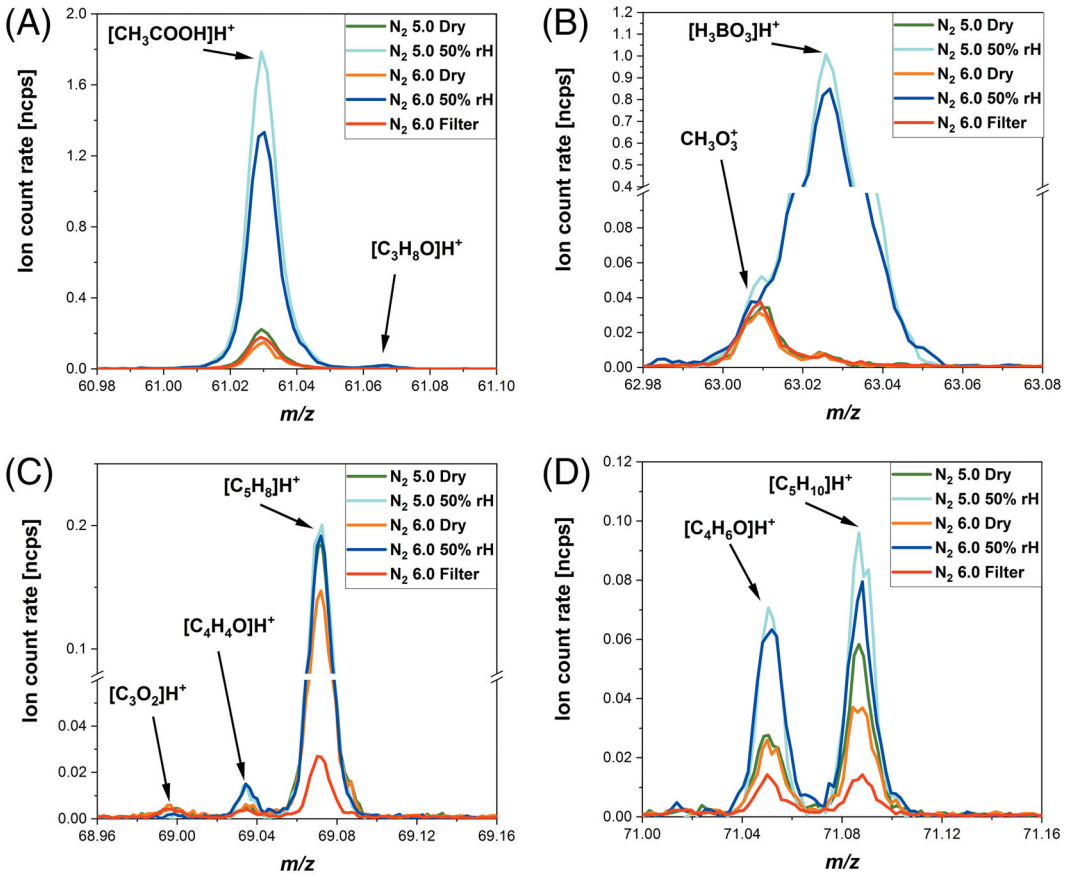

FIGURE 5 Comparison of the profile mass spectra of selected ions (A) $[C_2H_4O_2]H^+$, (B) $[HBO_2]H_3O^+$, (C) $[C_5H_8]H^+$, and (D) $[C_5H_{10}]H^+$ measured in nitrogen background under dry and humid conditions (50% relative humidity [RH] at 20°C) using H_3O^+ as primary ion in a proton transfer reaction quadrupole interface time-of-flight mass spectrometer (PTR-QiTOF) at a reduced electric field (E/N) of 131 Td

ethanethiol ($[C_2H_6S]H^+$) at *m/z* 63.026 could also be ruled out because the second most abundant isotope does not fit to the isotopic pattern. Because of the high resolution of the PTR-QiTOF, the [M]H_3O^+ association ion of acetaldehyde (*m/z* 63.044) could also be ruled out. In order to corroborate the presumed origin of the $[H_3BO_3]H^+$ ion, a comparison with commercial high-performance liquid chromatography (HPLC)-grade water was carried out (Figure S3a). It could be shown that the origin of this compound is independent of the water origin but can be related to the DURAN® bottles used for humidification. The storing time seems to play a role on the concentration of this boron species due to its diffusion from the glass into water, but more exhaustive analysis is out of the scope of this study. An origin of the compound in the gas calibration system itself can be excluded as in this case, similar signals for both water sources can be expected.

At *m/z* 69 (Figure 5C), three isobaric peaks were found, which could be assigned to the $[C_3O_2]H^+$, $[C_4H_4O]H^+$, and $[C_5H_8]H^+$ ions. The $[C_3O_2]H^+$ ion at *m/z* 68.997 appears as an instrument artifact without clear humidity dependency. The PA of C_3O_2 was reported to be >727 kJ mol^{-1}, and the heat of formation of the protonated molecule was <709 kJ mol^{-1}.[84] The $[C_4H_4O]H^+$ ion at *m/z* 69.033 has been assigned to furan, which appears to be a gas impurity and a memory effect. It exhibits a positive humidity dependency with a signal increase of about 3.6 and 2.6 for N_2 5.0 and N_2 6.0, respectively. A contribution to this ion could originate from the dehydrogenation of the $[C_4H_6O]H^+$ ion (Figure 5D), here assigned as 2,5-dihydrofuran. Furan has been reported in environmental studies,[75,85] in confined plumes[86] and with thermal desorption coupled to gas chromatography–mass spectrometry (TD-GCMS) to be only present in biogases from biogas plants with dry fermentation but not with wet fermentation.[1] Additionally, it has also been reported in a PTR-TOF-MS analysis of biogas.[87] A good separation from the isobar isoprene was first achieved by Jordan et al.[88] thanks to improved mass resolution.

The $[C_5H_8]H^+$ ion at *m/z* 69.070 (Figure 5C) is mainly reported as isoprene in breath analysis,[18,89] environmental studies,[18,21,49,90] and food analysis[91] but less common as cyclopentene.[85] In this study, the $[C_5H_8]H^+$ ion appears as gas impurity and memory effect with a signal reduction after filtering of about 81%. This ion does not exhibit a clear humidity dependency. This is in agreement with previous studies,[78,92] although it was also shown that at low E/N values, the humidity dependency becomes significant and has a negative trend. According

to Španěl and Smith[93] due to the exceptionally high PA of isoprene, it can react with the monohydrate $[H_2O]H_3O^+$ ion to form a weakly bound association ion, which later thermally dissociates (10 kJ mol^{-1}) to form $[C_5H_8]H^+$ plus H_2O at the end of the drift tube, before reaching the detector. Here, the $[C_5H_8]H^+$ ion is assigned to cyclopentene because isoprene has been reported to fragment to $C_3H_5^+$ (*m/z* 41.039),[92] which in this study seems not to correlate due to the different trend after filtering and the strong humidity dependency of the peak at *m/z* 41.039.

At *m/z* 71 (Figure 5D) two isobaric ions were found. The first one at *m/z* 71.049 was assigned as $[C_4H_6O]H^+$ and can be ascribed to 2,5-dihydrofuran. The second one at *m/z* 71.086 was assigned to $[C_5H_{10}]H^+$ and attributed to *trans*-2-pentene. Cyclopentane would have been considered if a correlation with cyclopentene could have been established but that is not the case. The former peak was categorized as gas impurity and memory effect with a positive humidity dependency, accounting for a signal increase of about 1.8 times. The latter one was equally assigned as gas impurity and memory effect with a positive humidity dependency with a signal increase under humid conditions of about 81% and 99% for N_2 5.0 and N_2 6.0, respectively. The peak at *m/z* 71 has been regarded as a fragment of larger molecules,[22,48,94] assigned as cyclopentane[66] and pentenes.[95]

At *m/z* 73 (Figure 6A), three isobaric ions were observed. The peak at *m/z* 73.028 was assigned to the $C_2H_5COO^+$ ion, at *m/z* 73.050 to the nearly incommensurable water cluster $[(H_2O)_3]H_3O^+$, and at *m/z* 73.065 to the $[C_4H_8O]H^+$ ion. The peak at *m/z* 73.028 has been observed before but was not identified.[88] Later, it was assigned to acrylic acid or methylglyoxal in emissions from biomass burning.[57] Here, this ion can been ascribed as a fragment of propanoic acid (Figure 6B). However, its dehydrogenation product acrylic acid $[C_2H_3COOH]H^+$ would also be possible. It was categorized as artifact with a positive humidity dependence accounting for a signal increase of about six times under humid conditions. The water cluster $[(H_2O)_3]H_3O^+$ exhibits a small increase under humid conditions of only 45%. The $[C_4H_8O]H^+$ ion has been reported as 2-butanone.[69] However, tetrahydrofuran is also a plausible isomer, and the presence of 2,5-dihydrofuran indicates again a possible dehydrogenation taking place in the drift tube. The profiles after filtering support this assumption. This ion appears as gas impurity and memory effect with a positive humidity dependency of about 74% for N_2 5.0.

Two isobaric peaks at *m/z* 75 with a similar humidity dependency are shown in Figure 6B, which are equally assigned as artifacts. The first peak was associated with a fragment $(CH_3)_2OHSi^+$ (*m/z* 75.026), possibly originating from trimethylsilanol after losing a methyl group.

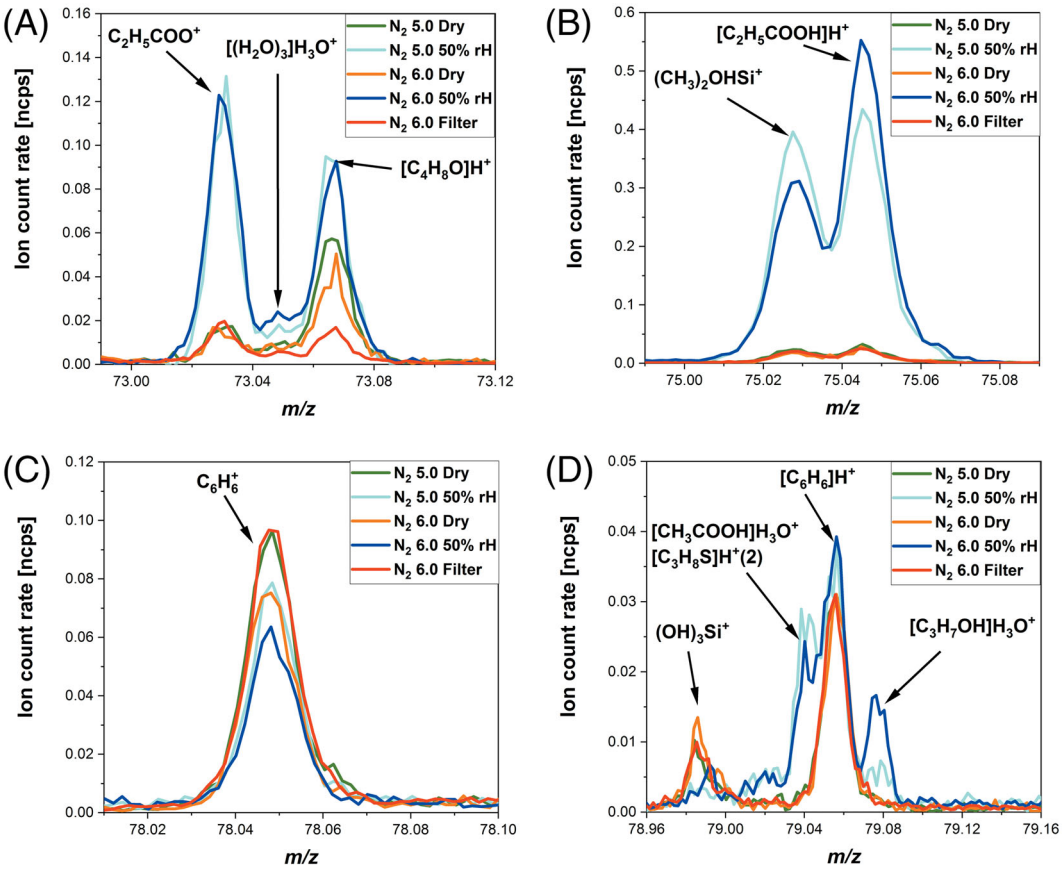

FIGURE 6 Comparison of the profile mass spectra of selected ions (A) $[C_3H_5O_2]H^+$, (B) $[C_3H_6O_2]H^+$, (C) $C_6H_6^+$, and (D) $[C_6H_6]H^+$, measured in nitrogen background under dry and humid conditions (50% relative humidity [RH] at 20°C) using H_3O^+ as primary ion in a proton transfer reaction quadrupole interface time-of-flight mass spectrometer (PTR-QiTOF) at a reduced electric field (E/N) of 131 Td

However, a correlation to the expected peak for trimethylsilanol at *m/z* 91.057 was not observed. Although as shown later in Figures 9 and 10, siloxanes were found in the nitrogen background, which eventually could generate this fragment, they do not exhibit a negative humidity dependency. The remarkably high positive humidity dependency (a factor of ~20 times) is ascribed to a possible hydrolysis reaction of the Sulfinert® coating of the evaporator and the piping lines used, which under humid conditions undergo an enhanced stripping effect from water. In order to confirm this hypothesis, comparison experiments were carried out with three different lines connecting the calibration gas generator and the PTR-QiTOF. The pipelines used were of PTFE, Sulfinert® coated, and uncoated steel, which were heated at 150°C. The results are shown in Figure S4a. It was observed that the nature of the inlet has a significant influence on the measured signals. Under dry conditions, PTFE appears to perform better (PTFE > Sulfinert® > steel) due to less wall adsorption effects, showing a peak reduction between PTFE and steel of 59.4%, which implies that for the fragment generating the $(CH_3)_2OHSi^+$ ion, the approximately 2.5-m inlet line itself has little contribution and its origin lies inside the calibration gas generator. However, under humid conditions, PTFE and steel perform similar, but Sulfinert® exhibits a signal increase of 133.8%, indicating an additional contribution from the Sulfinert® line. The second peak at *m/z* 75 in Figure 6B is assigned as propanoic acid $[C_2H_5COOH]H^+$ (*m/z* 75.044), which appears as artifact and exhibits a positive humidity dependency with a signal increase of about 16 and 24 times for N_2 5.0 and N_2 6.0, respectively. Its origin is presumed to be a decomposition product of some polymer material or glued parts in the PTR-QiTOF. This peak has been reported as a fragment of larger esters,[96] 3-hydroxy-propanal,[22] hydroxyacetone, methyl acetate, ethyl formate, and a decomposition product of 4-hydroxy-butanal.[57] If this ion is a fragment of larger esters, a higher intensity would be expected under dry conditions. From all isomers, propanoic acid seems most likely due to the presence of acrylic acid.

Figure 6C shows the $C_6H_6^+$ ion, which usually does not receive much attention, because it is assumed that benzene protonates to 100%. However, its presence in our system suggests some charge transfer reaction, most likely with NO^+ or O_2^+, but as previously shown,[43] they contributed to the total ion in our system with only 0.2%. However, it can also be generated by the fragmentation of higher aromatic compounds (e.g., toluene, ethylbenzene, and xylenes), which under dry conditions like those after filtering could be favored. This peak shows a slight negative humidity dependency of about 21% and 24% for N_2 5.0 and N_2 6.0, respectively. Although the lower intensity of $C_6H_6^+$ ion in N_2 6.0 under dry condition compared with N_2 5.0 is expected, it remains unclear why the protonated molecule (Figure 6D) appears as artifact but with a slightly positive humidity dependency of about 15% and 18% for N_2 5.0 and N_2 6.0, respectively, in contrast to previous results.[78] At *m/z* 79, five isobaric contributions are observed. The $(OH)_3Si^+$ ion appears as artifact with negative humidity dependency of about 43% and 49% for N_2 5.0 and N_2 6.0, respectively. A plausible origin for this ion would be the subsequent substitution of the CH_3 groups by OH groups in the $(CH_3)_2OHSi^+$ ion. In Figure S4b, a similar trend was observed for the three inlet materials: PTFE, Sulfinert®, and steel. This suggests that the origin of this ion may be inside the PTR-QiTOF. The interference of hydrated acetic acid ($[CH_3COOH]H_3O^+$) at *m/z* 79.039 with benzene has been reported before.[68,97] At about the same *m/z*, the second most abundant isotope of sulfur compounds with the chemical formula $[C_3H_8S]H^+$(2) (*m/z* 79.038) would interfere with the benzene signal. Plausible assignments to the $[C_3H_8S]H^+$ ion are propanethiols[87] or ethylmethylsulfide.[98] Due to the remarkably positive humidity dependency of about 10 times, this peak can be assigned to the hydrated acetic acid. At *m/z* 79.075, another association ion was observed to interfere with benzene. This peak was assigned to the $[C_3H_7OH]H_3O^+$ ion, which is attributed to hydrated propanols.[99] These interferences have a big impact in the analysis of benzene in process gases like biogases and can obscure quantitative assessments, because such gases are typically rich in acetic acid, sulfur compounds, and propanols and additionally are saturated with water vapor,[1] which would favor the formation of association clusters. Therefore, their eventual contribution to the benzene signal should be taken into account.

3.4 | Mass range *m/z* 80–100

Figure 7A shows two isobaric ions at *m/z* 81. The first one at *m/z* 81.037 was assigned to the association ion $[H_3BO_3]H_3O^+$ (*m/z* 81.035). This artifact is nearly unmeasurable under dry conditions and exhibits a remarkable positive humidity dependency with a signal increase of factor of 44 times. This ion has not been reported before in PTR measurements and confirms the assignment of the peak at *m/z* 63.025. Similarly to the $[H_3BO_3]H^+$ ion, the origin of this ion was corroborated with the comparison measurement using HPLC-grade water and is shown in Figure S3b. The peak at *m/z* 81 has commonly been assigned as fragment of terpenes,[100–102] cyclohexanol,[47] and aldehydes.[22,46] The second isobaric peak was assigned to the $[C_6H_8]H^+$ ion (*m/z* 81.070), which was categorized as gas impurity and memory effect with a positive humidity dependency, accounting for a signal increase of about 35% and 90% for N_2 5.0 and N_2 6.0, respectively. This peak was attributed to cyclohexadiene, possibly a dehydrogenation product of cyclohexene. At *m/z* 83 (Figure 7B), two isobaric ions were assigned as gas impurities and memory effect. The first one was attributed to $[C_5H_6O]H^+$ at *m/z* 83.049, which is assigned to 3-methylfuran. It shows a positive humidity dependency with a signal increase of 2.3 times. The second isobar was assigned to cyclohexene $[C_6H_{10}]H^+$ at *m/z* 83.086. It shows no clear humidity dependency but a clear reduction after filtering of 77%. This peak has been assigned as a fragment of hexenols or hexanal.[103] However, the signal of the possible parent peak at *m/z* 101.096 does not correlate. At *m/z* 85 (Figure 7C), three isobars are observed: two with clear positive humidity dependencies and one with a less clear trend. The first one was categorized as artifact and assigned to $[C_4H_4O_2]H^+$ (*m/z* 85.028) with a signal increase under humid conditions of about 2.7 times. It is ascribed to 1,4-dioxin, a possible dehydrogenation

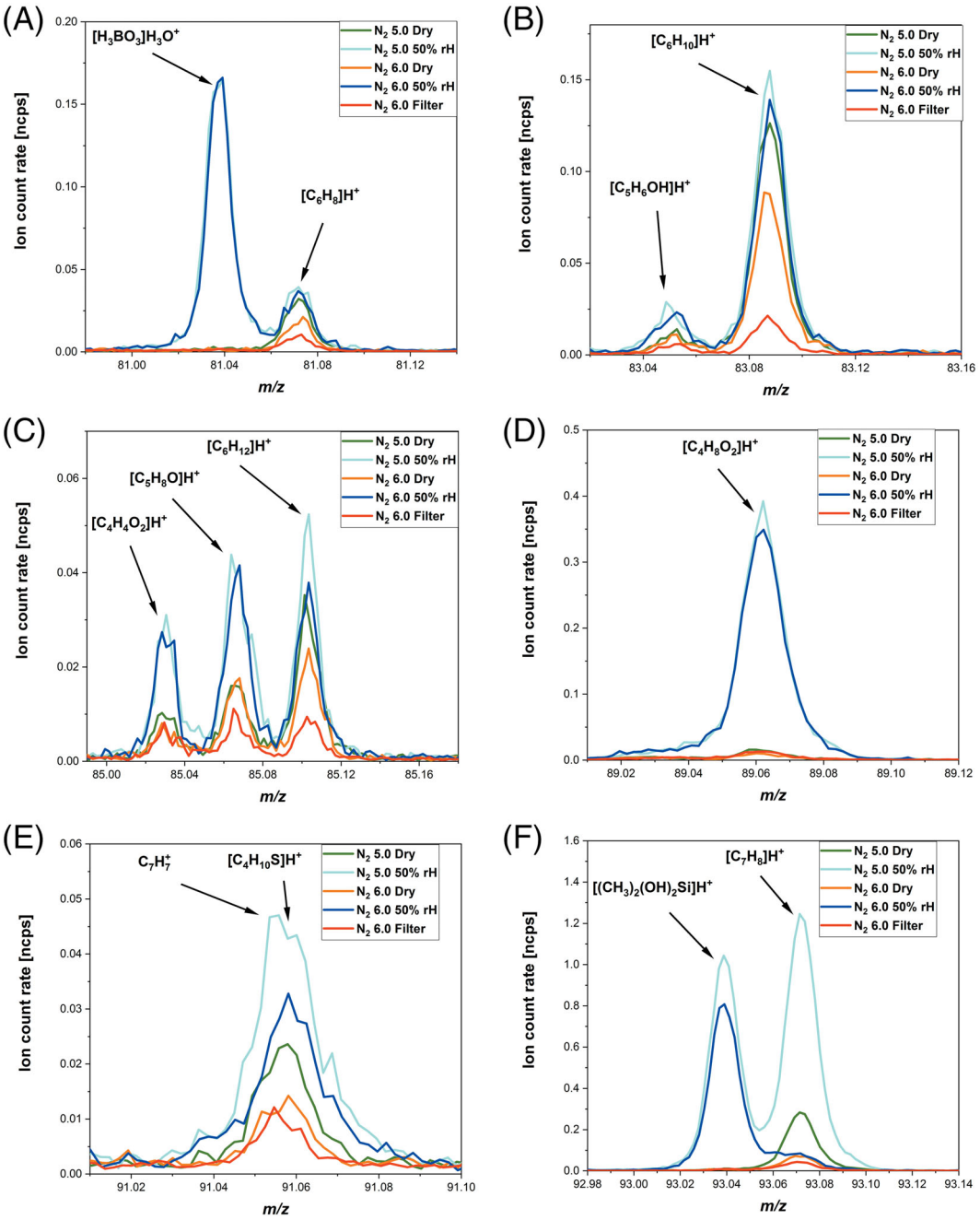

FIGURE 7 Comparison of the profile mass spectra of selected ions (A) $[HBO_2][H_2O]H_3O^+$, (B) $[C_6H_{10}]H^+$, (C) $[C_6H_{12}]H^+$, (D) $[C_4H_8O_2]H^+$, (E) $[C_4H_{10}S]H^+$, and (F) $[C_7H_8]H^+$, measured in nitrogen background under dry and humid conditions (50% relative humidity [RH] at 20°C) using H_3O^+ as primary ion in a proton transfer reaction quadrupole interface time-of-flight mass spectrometer (PTR-QiTOF) at a reduced electric field (E/N) of 131 Td

product of 1,4-dioxane. It has been reported as 2-furanone[104] and pentenone.[58] The second isobar was assigned to cyclopentanone $[C_5H_8O]H^+$ (*m/z* 85.065), which exhibits a positive humidity dependency with a signal increase of about 2.7 times. The third isobar was assigned to $[C_6H_{12}]H^+$ (*m/z* 85.101) and ascribed to cyclohexane. It has already been reported as 2-methyl-2-pentene/*trans*-2-hexene/cyclohexane.[66] Its signal increase under humid conditions accounts for 45% and 70% for N_2 5.0 and N_2 6.0, respectively. In Figure 7D, the peak was assigned to $[C_4H_8O_2]H^+$ (*m/z* 89.060), probably 1,4-dioxane. It appears as an artifact with a remarkably high humidity dependency with a signal increase under humid condition of a factor of 21 times. The peak at *m/z* 89 has been previously ascribed to 2-methyl-1,3-dioxolane or butyric acid.[105] Figure 7E shows a peak at *m/z* 91 with positive humidity dependency, which appears to be a gas impurity and memory effect. Figure 7E shows only two tentative assignments; however, at this *m/z*, the following isobars can contribute to the signal: $C_7H_7^+$,[82] $[C_3H_9OHSi]H^+$ (trimethylsilanol), $[C_4H_{10}S]H^+$ (diethyl sulfide/butanethiol),[87] and $[(H_2O)_4]H_3O^+$.[78] It remains

unclear which compounds contribute to this signal, because $C_7H_7^+$ does not correlate with toluene and for trimethylsilanol and diethyl sulfide a differentiation cannot be made. The ion at *m/z* 91 has been reported to be the result of the association of the $(CH_3)_3Si^+$ ion (*m/z* 73.047) with water,[106,107] which here was incommensurable and, if present, the small signal overlapped with the water cluster $[(H_2O)_3]H_3O^+$. In SIFT-MS measurements using H_3O^+, trimethylsilanol was shown to give the ion at *m/z* 91.057, and in the presence of water, it converts to $(CH_3)_2SiOH.(H_2O)^+$ at *m/z* 93.037, $(CH_3)_3Si.(H_2O)_2^+$ at *m/z* 109.068, and $(CH_3)_2SiOH.(H_2O)_2^+$ at *m/z* 111.047.[108] Figure 7F shows the well-known peak at *m/z* 93.070 for protonated toluene $[C_7H_8]H^+$.[78,109] Surprisingly, also, an isobar at *m/z* 93.039 assigned as $[(CH_3)_2(OH)_2Si]H^+$ (*m/z* 93.037) was observed, which under humid conditions exhibits a signal increase with a factor of about 53 and 90 times for N_2 5.0 and N_2 6.0, respectively. In our case, no correlation between the ions at *m/z* 91 and *m/z* 93 is observed, indicating a different origin. Analogous to $(CH_3)_2OHSi^+$, the appearance of the peak at *m/z* 93.039 under humid conditions suggests some kind of surface hydrolysis of the Sulfinert® coating of the pipelines. In the comparison of the inlets shown in Figure S4c, this ion shows a similar trend with all three inlets, which suggests that it may originate from inside the calibration gas generator or the PTR-QiTOF. Toluene exhibits a very peculiar trend; in N_2 5.0, a positive humidity dependency is observed with a signal increase of about 4.6 times, whereas in N_2 6.0, no clear humidity dependency can be established. Because N_2 5.0 is less clean than N_2 6.0, it would be plausible that in N_2 5.0, some contribution to the toluene signal comes from fragments of larger molecules. In Figure S4c an unexpected trend of the signals of toluene under dry and humid conditions was observed (steel > PTFE > Sulfinert®). For inert materials like PTFE and Sulfinert®, higher signals are expected as a result of smaller losses caused by wall adsorption effects. This indicates that the higher signals observed with uncoated steel are the result of contributions from fragmentation of larger aromatic compounds, which for steel in comparison with Sulfinert® coated lines shows a signal increase of about 3.3 times for dry and humid conditions.

3.5 | Mass range > *m/z* 100

Figure 8A shows three isobars at *m/z* 121: $[C_4H_8O_2S]H^+$, $[C_8H_8O]H^+$, and $[C_9H_{12}]H^+$. For $[C_4H_8O_2S]H^+$ (*m/z* 121.032), it is not clear if it is an artifact or a gas impurity. It exhibits a positive humidity dependency (~2.3 times). The $[C_8H_8O]H^+$ (*m/z* 121.065) ion has been previously attributed to vinylphenol, but it can be discarded here due to its biological nature and, therefore, was assigned as acetophenone.[58] Its positive humidity dependency accounts for a signal increase of 2.9 times. The $[C_9H_{12}]H^+$ (*m/z* 121.101) ion is commonly assigned to C9 aromatics,[110] and it is assigned here to 1,2,4-trimethylbenzene. It exhibits a positive humidity dependency (~58% signal increase). This peak was categorized as gas impurity and memory effect. Figure 8B shows a peak at *m/z* 123 with a significant positive humidity dependency (10.5 times increase), assigned as $[C_7H_6O_2]H^+$ (*m/z* 123.044), which has been previously reported as salicyladehyde.[57] Here, it is tentatively assigned as benzoic acid. The $[C_9H_{14}]H^+$ ion (*m/z* 123.117) is likely to be a product of $[C_9H_{16}]H^+$ (Figure 8C) after losing a H_2. The $[C_9H_{16}]H^+$ ion (*m/z* 125.133) has been reported as nonadiene.[111] It appears as a gas impurity and memory effect. After filtering, its signal reduces about 81%. Its positive humidity dependency accounts for about 28% increase. At *m/z* 129, three isobars can be identified (Figure 8D). The first one is the $[C_{10}H_8]H^+$ ion (*m/z* 129.070) associated to naphthalene.[57] Here, this peak appears as gas impurity and memory effect with a small positive humidity dependency. It overlaps with a peak associated to $[C_7H_{12}O_2]H^+$ (*m/z* 129.091), which becomes visible under humid conditions and exhibits a significant signal increase of about 6.9 times. It has been previously measured in PTR instruments.[110] The $[C_8H_{16}O]H^+$ ion[110] (*m/z* 129.127) appears here as gas impurity with nearly no memory effect and a positive humidity dependency (Factor 2). The formation of the $[C_7H_{12}O_2]H^+$ ion under humid conditions suggests a similar mechanism as for the silicon-organic compounds for the $[C_8H_{16}O]H^+$ ion by exchanging a CH_3 group for an OH group but with a subsequent dehydrogenation. For the $[C_{11}H_{10}]H^+$ ion (*m/z* 143.086), a similar trend was observed (Figure 8E), previously associated to methylnaphthalenes.[58] Here, it appears as gas impurity and memory effect with no clear humidity dependency. It overlaps with the $[C_8H_{14}O_2]H^+$ ion (*m/z* 143.107) under humid conditions. Again, this latter ion could form by the exchange of a CH_3 group for an OH group in the $[C_9H_{18}O]H^+$ ion (nonanal[74]) followed by a dehydrogenation step. The latter appears as gas impurity with nearly no memory effect and exhibits a positive humidity dependency with a signal increase of about 52%. At *m/z* 155.086, this pattern repeats for the $[C_{12}H_{10}]H^+$ ion (Figure 8F), associated with acenaphthene. This peak is assigned as gas impurity with low memory effect and with no clear humidity dependency. It overlaps with the $[C_9H_{14}O_2]H^+$ ion (*m/z* 155.107), which could be the product under humid conditions after exchanging a CH_3 group for an OH group with a subsequent dehydrogenation step from the $[C_{10}H_{18}O]H^+$ ion (*m/z* 155.143), which is associated to linalool.[112]

3.6 | Mass range *m/z* 160 upwards: Siloxanes

At high masses, in the spectra of the nitrogen background, siloxanes were observed. Figure 9C shows a peak at *m/z* 163.097 associated to the linear hexamethyldisiloxane ($[C_6H_{18}OSi_2]H^+$), also known as L2. L2 is commonly found in landfill gas[108,113,114] and in biogases.[1,115] The $[C_6H_{18}OSi_2]H^+$ ion appears as gas impurity with nearly no memory effect after filtering. It exhibits a positive humidity dependency, accounting for about 37% increase in signal. In electron impact ionization of L2, the two major fragment ions produced are $Si_2OC_5H_{15}^+$ at *m/z* 147.066 and $Si_2OC_4H_{11}^+$ at *m/z* 131.034.[116] The peak at *m/z* 147.066 (Figure 9A) is assigned to the product $C_5H_{15}OSi_2^+$ as a result of losing a methyl group. This mechanism appears to be favored under dry conditions. The loss of a methyl group has been reported for the siloxane D5 but not for L2.[110] In this

study, the $Si_2OC_4H_{11}^+$ ion was not observed. In a SIFT-MS and PTR-MS study,[106] it was shown that in SIFT-MS, the main reaction channel results in the ion at *m/z* 147.066, whereas in PTR-MS, at an E/N of 140 Td, the main ion occurs at *m/z* 149.045, which is in agreement with our findings. The reaction channel producing the ion at *m/z* 149.045 corresponds to the exchange of a methyl group for an OH group, forming $C_4H_{13}O_2Si_2^+$. Under humid conditions, a signal drop of about 47% is observed. It was also shown that at low E/N, protonated L2 quickly undergoes secondary chemistry in the presence of water producing two significant ions at *m/z* 165.076 ($Si_2O(CH_3)_5(H_2O)^+$) and *m/z* 167.055 ($Si_2O(CH_3)_4(H_2O)_2^+$).[106,108] This is in contrast to our findings where only the hydrated ion $[C_4H_{12}O_2Si_2]H_3O^+$ at *m/z* 167.055 is observed under humid conditions (50% RH) showing a signal increase of about 4.5 times. For the symmetrical siloxane L2 the $[M]H_3O^+$ association ion was not observed, perhaps due its low dipole moment. In Figure 9C, a shoulder about *m/z* 163.140 becomes visible under humid conditions but remains unidentified.

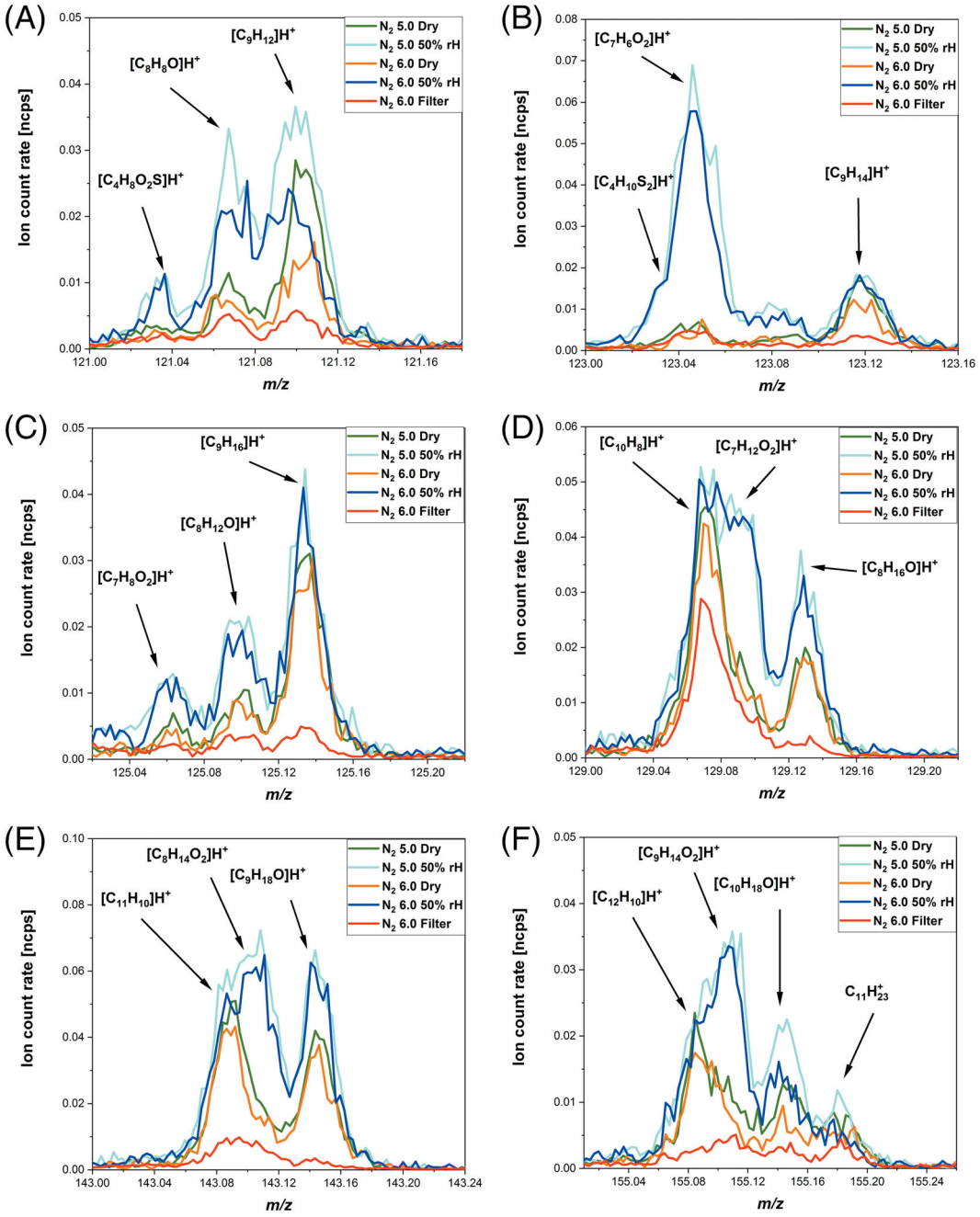

FIGURE 8 Comparison of the profile mass spectra of selected ions (A) $[C_9H_{12}]H^+$, (B) $[C_9H_{14}]H^+$, (C) $[C_9H_{16}]H^+$, (D) $[C_{10}H_8]H^+$, (E) $[C_{11}H_{10}]H^+$, and (F) $[C_{12}H_{10}]H^+$, measured in nitrogen background under dry and humid conditions (50% relative humidity [RH] at 20°C) using H_3O^+ as primary ion in a proton transfer reaction quadrupole interface time-of-flight mass spectrometer (PTR-QiTOF) at an reduced electric field (E/N) of 131 Td

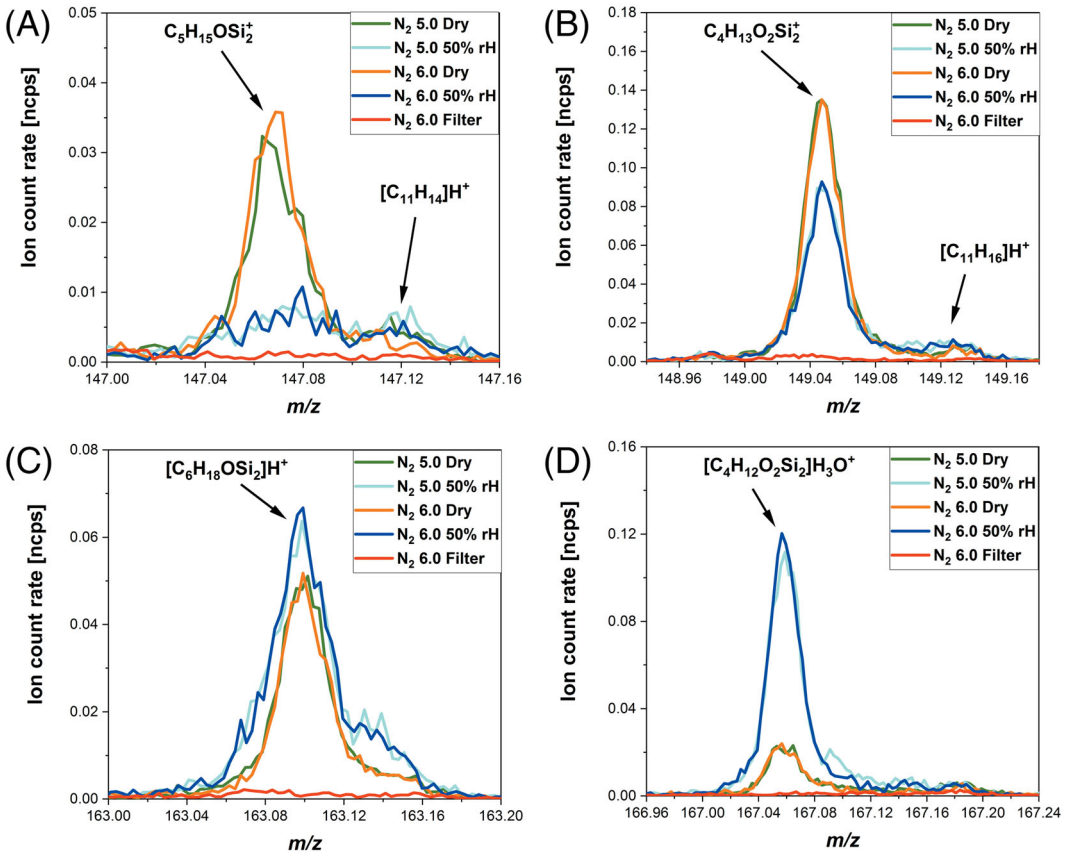

FIGURE 9 Comparison of the profile mass spectra of the siloxane hexamethyldisiloxane (L2) and some byproducts (A) $C_5H_{15}OSi_2^+$, (B) $C_4H_{13}O_2Si_2^+$, (C) $[C_6H_{18}OSi_2]H^+$, and (D) $[C_4H_{12}O_2Si_2]H^+$, measured in nitrogen background under dry and humid conditions (50% relative humidity [RH] at 20°C) using H_3O^+ as primary ion in a proton transfer reaction quadrupole interface time-of-flight mass spectrometer (PTR-QiTOF) at a reduced electric field (E/N) of 131 Td

Similarly to L2, cyclic siloxanes like hexamethylcyclotrisiloxane (D3), octamethylcyclotetrasiloxane (D4), and decamethylcyclopentasiloxane (D5) are also typically found in landfill gas[113,114] and biogas.[1,115] Siloxanes like D3 and D4 have been previously measured with SIFT-MS[108] and PTR-MS[40,87] and D5 with PTR-TOF-MS.[117] The loss of a methyl group for D5 has been reported.[110] The siloxanes D3 ($[C_6H_{18}O_3Si_3]H^+$) at *m/z* 223.064 and D4 ($[C_8H_{24}O_4Si_4]H^+$) at *m/z* 297.082 appear in this study as gas impurities, and in contrast to L2, both exhibited a slight memory effect (Figure 10A,C) after filtering. These two siloxanes show no clear humidity dependency. The respective $[M]H_3O^+$ ions were not observed. Figure 10B shows the product of the main reaction channel for the siloxane D3 by the exchange of the methyl group for a hydroxide group. Similarly, the siloxane D4 exhibits the same reaction channel in Figure 10D.

3.7 | Compound class distribution

In the nitrogen background measurements, 1140 peaks were observed. According to the criterion applied for the peak assignment, that a peak must possess an intensity of at least 3σ higher than the average noise level, 674 peaks were selected. From these, only 660 were considered for the analysis because the primary ion, water clusters, and some fragments were discarded. From the 660 peaks, 463 tentative chemical formulas for the main isotopes could be assigned and only 45 peaks remained unidentified. Among these 660 peaks, 337 could be identified as instrument or setup artifacts, whereas 257 occur as VOCs in the nitrogen background, 12 originated from the filter and for 54 peaks an assignment as VOC or artifact remains unclear. A complete list of all ions identified and considered in this study is given in Tables S1 and S2. Table S1 shows a qualitative assignment of the peaks in the nitrogen mass spectrum as artifact, VOC (gas impurity), from filter or unclear. Table S2 shows a qualitative assignment of the peaks regarding their measurability under dry and humid conditions and their positive or negative humidity dependencies.

Figure 11 shows the compound class distribution according to the following classification based on the chemical formulas assigned:

- O-containing (metallic): are compounds such as metal oxides and hydroxides.
- O-containing (nonmetallic): are organic compounds such as alcohols, aldehydes, ketones, carboxylic acids, and esters.

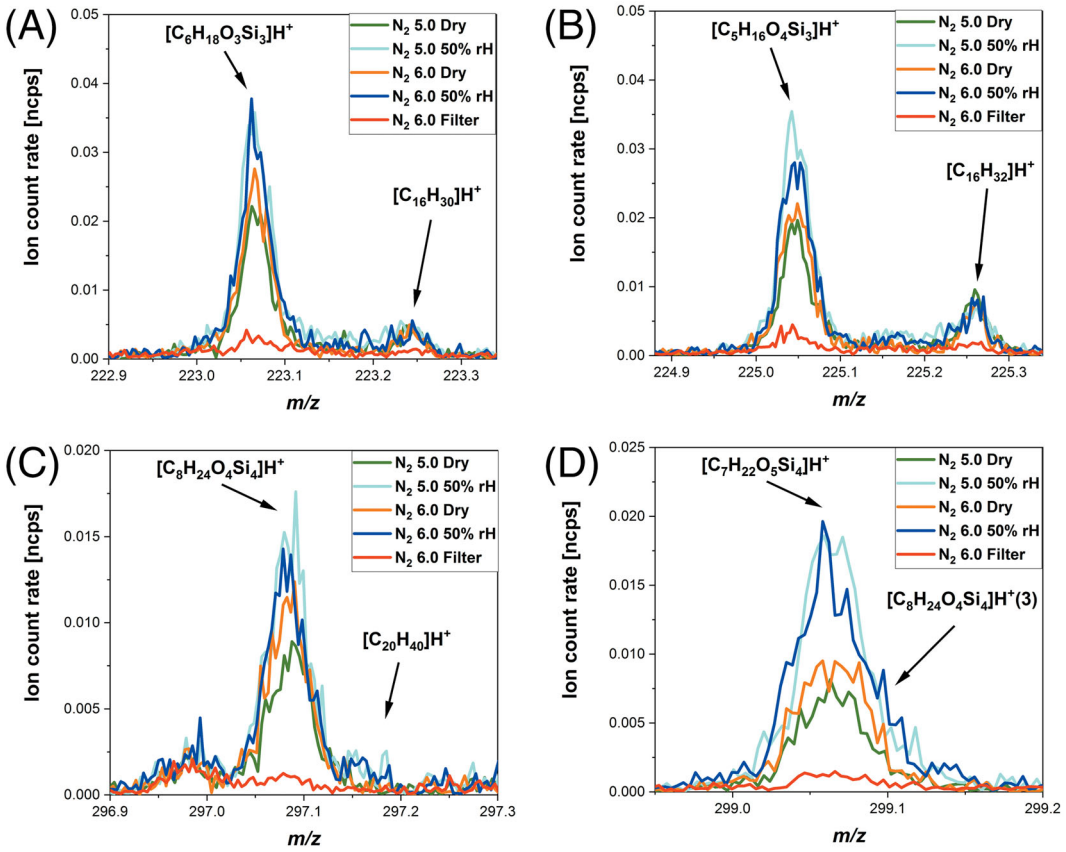

FIGURE 10 Comparison of the profile mass spectra of the siloxanes hexamethylcyclotrisiloxane (D3) and octamethylcyclotetrasiloxane (D4) and some byproducts (A) $[C_6H_{18}O_3Si_3]H^+$, (B) $[C_5H_{16}O_4Si_3]H^+$, (C) $[C_8H_{24}O_4Si_4]H^+$, and (D) $[C_7H_{22}O_5Si_4]H^+$, measured in nitrogen background under dry and humid conditions (50% relative humidity [RH] at 20°C) using H_3O^+ as primary ion in a proton transfer reaction quadrupole interface time-of-flight mass spectrometer (PTR-QiTOF) at a reduced electric field (E/N) of 131 Td

- S-containing: are inorganic and organic compounds containing sulfur.
- N-containing: are organic compounds such as amines, amides, and nitriles. The contribution from the main parasitic ions such as $[NH_3]H^+$, N_2^+, $[N_2]H^+$, NO^+, HN_3^+, and N_4^+ and their respective isotopes was not considered.
- Si-containing: are mainly silicon-organic compounds and their fragments.
- Metallic: are the metallic ions such as Fe^+, Ni^+, and Cr^+.
- Other nonmetals: are for instance halogenated and boron compounds.
- Hydrocarbons: are aliphatic, aromatic, and polyaromatic compounds.
- Unidentified: are the peaks for which a chemical formula could not be assigned.

In Figure 11A, it can be seen that the main contribution of peaks in the PTR mass spectrum of nitrogen can be ascribed to hydrocarbons and O-containing (nonmetallic) compounds with a contribution of 24.1% and 23.5%, respectively. The lowest contribution was from metal ions accounting for 2.7%. The unidentified peaks accounted only for 6.8%, which means that 93.2% of the peaks in the background measurements could be assigned. Regarding the 257 trace impurities identified in the nitrogen gases 5.0 and 6.0 (Figure 11B), it was found that the same VOCs were present in these gases but only their concentrations were different. The main contribution to the VOCs was from hydrocarbons, accounting for 50.2%, followed by nonmetallic oxygen-containing and silicon-containing compounds with a contribution of 30.7% and 11.3%, respectively. Only 1.9% of the peaks classified as VOCs remained unidentified.

In Figure 12, the ion intensities for the measurements of nitrogen 5.0 and 6.0 under dry and humid conditions without filtering were normalized to the O-containing (nonmetallic) signal, and for the filtered nitrogen 6.0, the ion intensities were normalized to the N-containing signal. In terms of ion intensity, the main contribution to the total ion signal (without primary ion and main artifacts) under dry conditions was from oxygen-containing (nonmetallic) compounds, closely followed by nitrogen-containing compounds (89% and 96% in nitrogen 5.0 and 6.0, respectively.), although after filtering, the nitrogen-containing compounds showed a signal increase of about 10%. However, if the nitrogen-containing parasitic

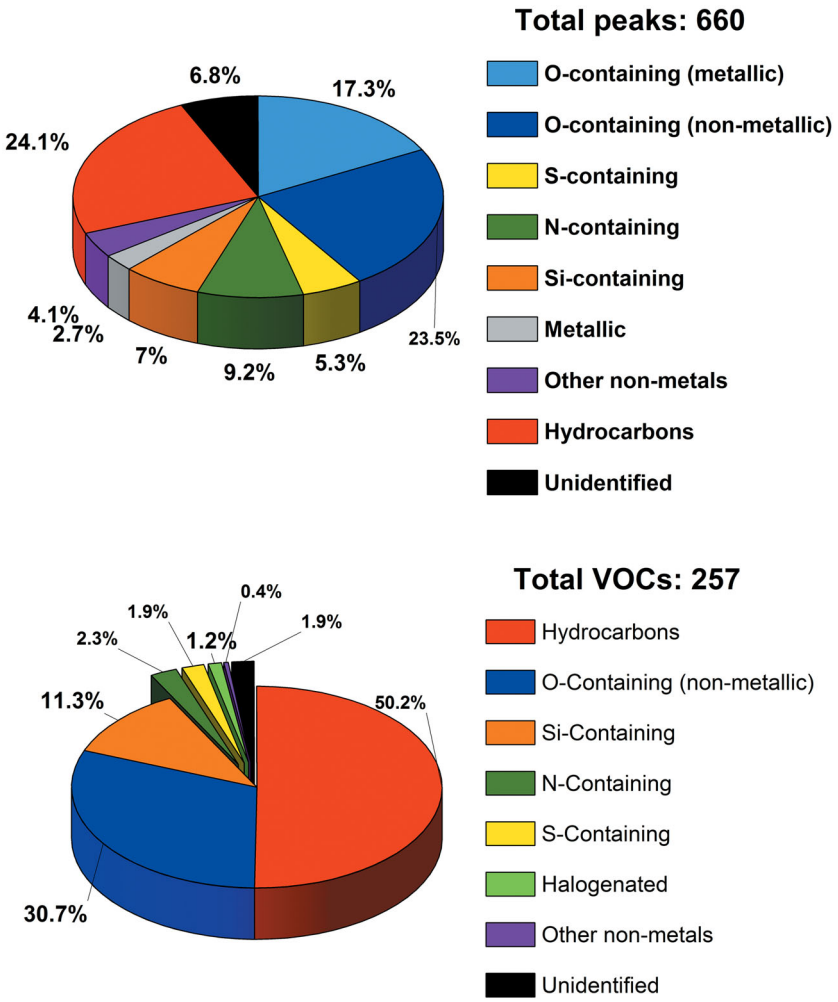

FIGURE 11 (A) Compound class distribution of the total number of peaks found in background measurements with pure nitrogen in a proton transfer reaction quadrupole interface time-of-flight mass spectrometer (PTR-QiTOF) under dry and humid conditions (50% relative humidity [RH] at 20°C) using H_3O^+ as primary ion at an reduced electric field [E/N] of 131 Td. (B) Compound class distribution of volatile organic compounds (VOCs) in nitrogen 5.0 and 6.0

ions (N^+, NH^+, NH_2^+, NH_3^+, $[NH_3]H^+$, N_2^+, $[N_2]H^+$, NO^+, N_3^+, N_4^+, etc.) would have been considered, the contribution to the total ion from N-containing compounds would have been more than 95%. Under humid conditions, the signal of oxygen-containing compounds exhibits a signal increment of 58% and 55% in N_2 5.0 and N_2 6.0, respectively. Another significant positive humidity dependency was observed for hydrocarbons, which showed a signal increase by a factor of 2.1 and 2.8 in N_2 5.0 and N_2 6.0, respectively. This is unexpected, because N_2 6.0 is in principle a purer gas than N_2 5.0. The positive humidity dependency is in contrast with previous results.[73] O-containing (metallic) compounds showed a relatively constant total signal in both regimes, perhaps as a result of the simultaneous vanishing of metal oxides and the formation of hydroxides, as previously shown.[43] Similarly, sulfur- and silicon-containing compounds showed a positive humidity dependency. On the other hand, it has been shown that under humid conditions less fragmentation takes place, and thus, the sensitivity of the protonated molecules increases.[46] For other nonmetals, a positive dependency with humidity was also observed. Metallic ions showed as expected a negative humidity dependency, and for the unidentified ions, no clear trend was observed.

4 | CONCLUSIONS

This work outlines the importance of the elucidation of the background in PTR measurements using pure nitrogen as gas matrix, especially for the case of nontarget analysis. A classification procedure helped the identification of new ions and their differentiation as gas impurity, memory effect, or artifact and established their humidity dependencies. Because PTR-MS cannot distinguish between the different origins of fragments and thus a direct identification is not possible, with the presented method, the origin of many fragments could be established. From 1140 peaks found in the mass range *m/z* 0–800, only 660 peaks were used for the analysis, from which 463 chemical formulas could be assigned in the mass spectrum and only 45 peaks remained unidentified. From these 660 peaks, 337 are related to instrument of setup artifacts, whereas 257 could be identified as VOCs in the nitrogen background. Based on this exhaustive analysis, a database will be built up, which can help the PTR community to identify unknown compounds and make aware of possible interferences and artifacts under dry and humid conditions. Humidity exhibited a big impact on the ion distribution showing that the highest contribution to the total ion signal for unfiltered nitrogen (5.0 and 6.0) under

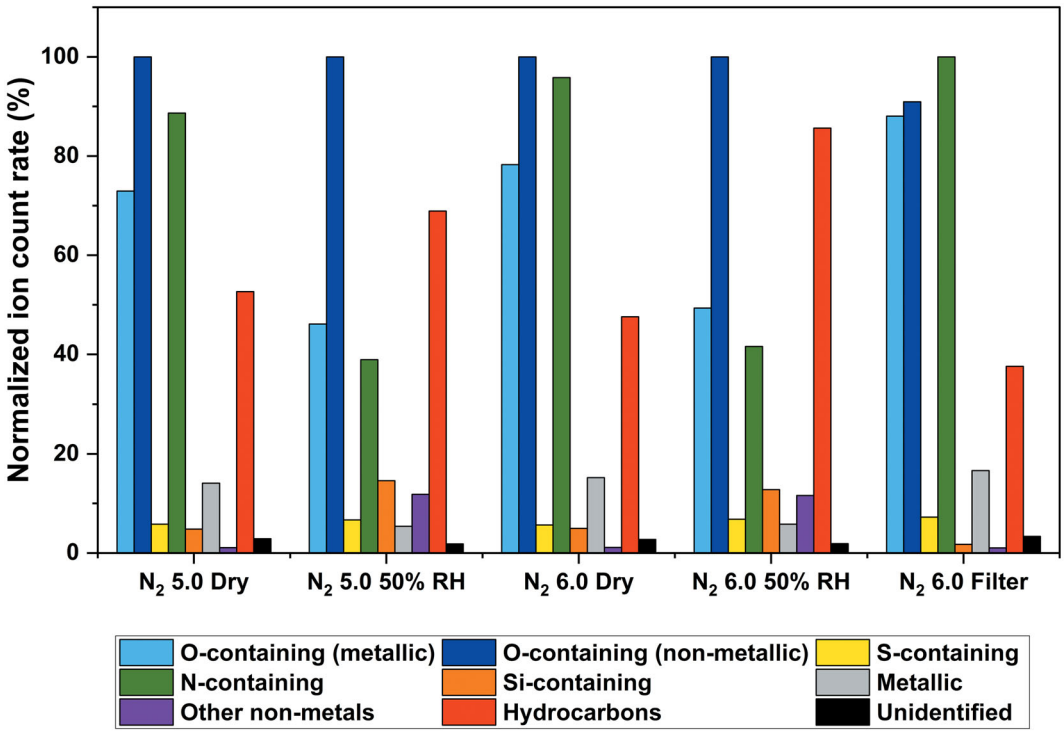

FIGURE 12 Normalized contributions to total ion of the 660 peaks found in background measurements with nitrogen in a proton transfer reaction quadrupole interface time-of-flight mass spectrometer (PTR-QiTOF) under dry and humid conditions (50% relative humidity [RH] at 20°C) using H_3O^+ as primary ion at a reduced electric field (E/N) of 131 Td

dry and humid conditions was from nonmetallic oxygenated compounds. However, under dry conditions, nitrogen-containing compounds exhibited the second highest contribution (normalized to nonmetallic oxygenated compounds) of 89% and 96% for nitrogen 5.0 and 6.0, respectively. The substitution of a CH_3 group by an OH group with or without subsequent dehydrogenation appears as a common reaction channel for many compounds in the drift tube of the PTR-QiTOF. In some cases, this reaction is favored under dry conditions (e.g., siloxanes) while in other cases, it is favored by humidity (e.g., oxygenated compounds). For the first time, S_x species were determined with PTR-TOF-MS and showed to form at room temperature in a reactive nickel-based filter. These findings and the elucidation of the mass spectrum up to *m/z* 800 pave the way for the interpretation of complex gas mixtures, such as metallurgical gases, where dilution with an inert carrier gas is necessary, thus avoiding misinterpretations and misestimations, which could have an impact on the design of purification systems or subsequent process designs.

ACKNOWLEDGEMENTS

The authors would like to thank the Max Planck Society for financial support as well as the Federal Ministry of Education and Research (in German: BMBF—Bundesministerium für Bildung und Forschung) for funding the projects HüGaProp (in German: Hüttengasproperties—wissenschaftliches Projekt zur Problematik der Verwendung von CO_2 Abgasströme aus dem Hochofen [Hüttengas] bei der Katalyse) Grant No. 03EK3546 and Carbon2Chem (Subproject L0) Grant No. 03EK3037C.

Open access funding enabled and organized by Projekt DEAL.

CONFLICT OF INTEREST

The authors declare no conflict of interest.

DATA AVAILABILITY STATEMENT

The data that support the findings of this study are available from the corresponding author upon reasonable request.

NOMENCLATURE

CCU	carbon capture and usage
cps	counts per second
E/N	reduced electric field
GC	gas chromatography
HPLC	high-performance liquid chromatography
MPV	multiport valve
PA	proton affinity
PEEK	polyether ether ketone
ppb_v	parts per million in volume
ppt_v	parts per trillion in volume
PTFE	polytetrafluoroethylene
PTR-MS	proton transfer reaction mass spectrometry
PTR-QiTOF	proton transfer reaction quadrupole interface time-of-flight mass spectrometer

PTR-TOF-MS	proton transfer reaction time-of-flight mass spectrometry
R	gas-phase analyte
RH	relative humidity
$[R]H^+$	protonated gas-phase analyte
SIFT	selected-ion flow tube
SIFT-MS	selected-ion flow-tube mass spectrometry
TD-GCMS	thermal desorption coupled to gas chromatography–mass spectrometry
VOCs	volatile organic compounds

ORCID

Jorge Iván Salazar Gómez https://orcid.org/0000-0002-6274-9530

Holger Ruland https://orcid.org/0000-0001-5530-1458

REFERENCES

1. Salazar Gómez JI, Lohmann H, Krassowski J. Determination of volatile organic compounds from biowaste and co-fermentation biogas plants by single-sorbent adsorption. *Chemosphere*. 2016;153:48-57.
2. Hashimoto S, Tanaka T, Yamashita N, Maeda T. An automated purge and trap gas chromatography-mass spectrometry system for the sensitive shipboard analysis of volatile organic compounds in seawater. *J Sep Sci*. 2001;24(2):97-103.
3. Saridara C, Brukh R, Mitra S. Development of continuous on-line purge and trap analysis. *J Sep Sci*. 2006;29(3):446-452.
4. Leidinger M, Schultealbert C, Neu J, Schutze A, Sauerwald T. Characterization and calibration of gas sensor systems at ppb level-a versatile test gas generation system. *Meas Sci Technol*. 2018;29(1):015901.
5. Sari S, Timo R, Jussi H, Panu H. Dynamic calibration method for reactive gases. *Meas Sci Technol*. 2020;31(3):034001.
6. Haerri HP, Macé T, Waldén J, et al. Dilution and permeation standards for the generation of NO, NO_2 and SO_2 calibration gas mixtures. *Meas Sci Technol*. 2017;28(3):035801.
7. Han JK, Liu XW, Chen D, Jiang M. Influence of relative humidity on real-time measurements of particulate matter concentration via light scattering. *J Aerosol Sci*. 2020;139:105462.
8. Helwig N, Schüler M, Bur C, Schütze A, Sauerwald T. Gas mixing apparatus for automated gas sensor characterization. *Meas Sci Technol*. 2014;25(5):055903.
9. Salazar Gómez JI, Takhtehfouladi ES, Schlögl R, Ruland H. Design and implementation of a gas generating system for complex gas mixtures and calibration gases. *Chem Ing Tech*. 2020;92(10):1574-1585.
10. Brunauer S, Emmett PH, Teller E. Adsorption of gases in multimolecular layers. *J Am Chem Soc*. 1938;60(2):309-319.
11. Sing KSW. Adsorption methods for the characterization of porous materials. *Adv Colloid Interface Sci*. 1998;76–77:3-11.
12. Leigh GJ. Haber-Bosch and other industrial processes. In: Smith BE, Richards RL, Newton WE, eds. *Catalysts for Nitrogen Fixation: Nitrogenases, Relevant Chemical Models and Commercial Processes*. Springer Netherlands; 2004:33-54.
13. Djozan D, Sorouraddin MH, Norouzi J, Farajzadeh MA. Sorbentless cryogenic needle trap device for the extraction of organic volatile compounds. *Microchim Acta*. 2012;177(1–2):81-88.
14. Yamanouchi T, Morimoto S, Honda H, et al. A new compact cryogenic air sampler and its application in stratospheric greenhouse gas observation at Syowa Station, Antarctica. *J Atmos Oceanic Tech*. 2009;26(10):2182-2191.
15. Suelves I, Lazaro MJ, Moliner R, Pinilla JL, Cubero H. Hydrogen production by methane decarbonization: Carbonaceous catalysts. *Int J Hydrogen Energy*. 2007;32(15):3320-3326.
16. Greene SA, Roy HE. Effect of different carrier gases on retention times in gas-adsorption chromatography. *Anal Chem*. 1957;29(4):569-570.
17. McGinitie TM, Karolat BR, Whale C, Harynuk JJ. Influence of carrier gas on the prediction of gas chromatographic retention times based on thermodynamic parameters. *J Chromatogr A*. 2011;1218(21):3241-3246.
18. Lindinger W, Hansel A, Jordan A. On-line monitoring of volatile organic compounds at pptv levels by means of proton-transfer-reaction mass spectrometry (PTR-MS) medical applications, food control and environmental research. *Int J Mass Spectrom Ion Processes*. 1998;173(3):191-241.
19. Hansel A, Jordan A, Holzinger R, Prazeller P, Vogel W, Lindinger W. Proton transfer reaction mass spectrometry: on-line trace gas analysis at the ppb level. *Int J Mass Spectrom Ion Processes*. 1995;149–150:609-619.
20. Lagg A, Taucher J, Hansel A, Lindinger W. Applications of proton transfer reactions to gas analysis. *Int J Mass Spectrom Ion Processes*. 1994;134(1):55-66.
21. Hayward S, Hewitt CN, Sartin JH, Owen SM. Performance characteristics and applications of a proton transfer reaction-mass spectrometer for measuring volatile organic compounds in ambient air. *Environ Sci Technol*. 2002;36(7):1554-1560.
22. D'Anna B, Wisthaler A, Andreasen O, et al. Atmospheric chemistry of C_3-C_6 cycloalkanecarbaldehydes. *J Phys Chem A*. 2005;109(23):5104-5118.
23. de Gouw J, Warneke C. Measurements of volatile organic compounds in the earth's atmosphere using proton-transfer-reaction mass spectrometry. *Mass Spectrom Rev*. 2007;26(2):223-257.
24. Yeretzian C, Jordan A, Lindinger W. Analysing the headspace of coffee by proton-transfer-reaction mass-spectrometry. *Int J Mass Spectrom*. 2003;223–224:115-139.
25. Romano A, Fischer L, Herbig J, et al. Wine analysis by FastGC proton-transfer reaction-time-of-flight-mass spectrometry. *Int J Mass Spectrom*. 2014;369:81-86.
26. Masi E, Romani A, Pandolfi C, Heimler D, Mancuso S. PTR-TOF-MS analysis of volatile compounds in olive fruits. *J Sci Food Agric*. 2015;95(7):1428-1434.
27. Biasioli F, Gasperi F, Odorizzi G, et al. PTR-MS monitoring of odour emissions from composting plants. *Int J Mass Spectrom*. 2004;239(2–3):103-109.
28. Clementschitsch F, Bayer K. Improvement of bioprocess monitoring: development of novel concepts. *Microb Cell Fact*. 2006;5(1):19.
29. Morken AK, Nenseter B, Pedersen S, et al. Emission results of amine plant operations from MEA testing at the CO_2 Technology Centre Mongstad. *12th International Conference on Greenhouse Gas Control Technologies, GHGT-12*. 2014;63:6023-6038.
30. Sanchez-Lopez JA, Zimmermann R, Yeretzian C. Insight into the time-resolved extraction of aroma compounds during espresso coffee preparation: online monitoring by PTR-ToF-MS. *Anal Chem*. 2014;86(23):11696-11704.
31. Herbig J, Gutmann R, Winkler K, Hansel A, Sprachmann G. Real-time monitoring of trace gas concentrations in syngas. *Oil Gas Sci Technol—Revue d'IFP Energies nouvelles*. 2013;69(2):363-372.
32. Agarwal B, Jurschik S, Sulzer P, et al. Detection of isocyanates and polychlorinated biphenyls using proton transfer reaction mass spectrometry. *Rapid Commun Mass Spectrom*. 2012;26(8):983-989.
33. Bukhtiyarov VI, Nizovskii AI, Bluhm H, et al. Combined in situ XPS and PTRMS study of ethylene epoxidation over silver. *J Catal*. 2006;238(2):260-269.
34. Knighton WB, Herndon SC, Franklin JF, et al. Direct measurement of volatile organic compound emissions from industrial flares using real-time online techniques: proton transfer reaction mass spectrometry and tunable infrared laser differential absorption spectroscopy. *Ind Eng Chem Res*. 2012;51(39):12674-12684.

35. Salazar Gómez JI, Klucken C, Sojka M, Waydbrink G, Schlögl R, Ruland H. The HüGaProp-Container: analytical Infrastructure for the Carbon2Chem® Challenge. *Chem Ing Tech*. 2020;92(10):1514-1524.
36. Han KH, Zhang JS, Guo B. Toward effective design and adoption of catalyst-based filter for indoor hazards: formaldehyde abatement under realistic conditions. *J Hazard Mater*. 2017;331:161-170.
37. Li JR, Zhang WP, Li C, Xiao H, He C. Insight into the catalytic performance and reaction routes for toluene total oxidation over facilely prepared Mn-Cu bimetallic oxide catalysts. *Appl Surf Sci*. 2021;550:149179.
38. Li JR, Zhang WP, Li C, He C. Efficient catalytic degradation of toluene at a readily prepared Mn-Cu catalyst: catalytic performance and reaction pathway. *J Colloid Interface Sci*. 2021;591:396-408.
39. Papurello D. Direct injection mass spectrometry technique for the odorant losses at ppb(v) level from nalophan™ sampling bags. *Int J Mass Spectrom*. 2019;436:137-146.
40. Papurello D, Tomasi L, Silvestri S. Proton transfer reaction mass spectrometry for the gas cleaning using commercial and waste-derived materials: focus on the siloxane removal for SOFC applications. *Int J Mass Spectrom*. 2018;430:69-79.
41. Graus M, Muller M, Hansel A. High resolution PTR-TOF: quantification and formula confirmation of VOC in real time. *J Am Soc Mass Spectrom*. 2010;21(6):1037-1044.
42. Blake RS, Whyte C, Hughes CO, Ellis AM, Monks PS. Demonstration of proton-transfer reaction time-of-flight mass spectrometry for real-time analysis of trace volatile organic compounds. *Anal Chem*. 2004;76(13):3841-3845.
43. Salazar Gómez JI, Klucken C, Sojka M, et al. Elucidation of artefacts in proton transfer reaction time-of-flight mass spectrometers. *J Mass Spectrom*. 2019;54(12):987-1002.
44. Deerberg G, Oles M, Schlögl R. The Project Carbon2Chem®. *Chem Ing Tech*. 2018;90(10):1365-1368.
45. Oles M, Luke W, Kleinschmidt R, et al. Carbon2Chem®—a cross-industry approach to reduce greenhouse gas emissions. *Chem Ing Tech*. 2018;90(1–2):169-178.
46. Pang X. Biogenic volatile organic compound analyses by PTR-TOF-MS: calibration, humidity effect and reduced electric field dependency. *J Environ Sci*. 2015;32:196-206.
47. Brown P, Watts P, Märk TD, Mayhew CA. Proton transfer reaction mass spectrometry investigations on the effects of reduced electric field and reagent ion internal energy on product ion branching ratios for a series of saturated alcohols. *Int J Mass Spectrom*. 2010;294(2–3):103-111.
48. Romano A, Hanna GB. Identification and quantification of VOCs by proton transfer reaction time of flight mass spectrometry: an experimental workflow for the optimization of specificity, sensitivity, and accuracy. *J Mass Spectrom*. 2018;53(4):287-295.
49. de Gouw JA, Goldan PD, Warneke C, et al. Validation of proton transfer reaction-mass spectrometry (PTR-MS) measurements of gas-phase organic compounds in the atmosphere during the New England Air Quality Study (NEAQS) in 2002. *J Geophys Res Atmos*. 2003;108(D21):4682.
50. Yuan B, Koss A, Warneke C, et al. A high-resolution time-of-flight chemical ionization mass spectrometer utilizing hydronium ions (H_3O^+ ToF-CIMS) for measurements of volatile organic compounds in the atmosphere. *Atmos Meas Tech*. 2016;9(6):2735-2752.
51. Thornberry T, Murphy DM, Thomson DS, et al. Measurement of aerosol organic compounds using a novel collection/thermal-desorption PTR-ITMS instrument. *Aerosol Sci Tech*. 2009;43(5):486-501.
52. Crespo E, Devasena S, Sikkens C, Centeno R, Cristescu SM, Harren FJ. Proton-transfer reaction mass spectrometry (PTRMS) in combination with thermal desorption (TD) for sensitive off-line analysis of volatiles. *Rapid Commun Mass Spectrom*. 2012;26(8):990-996.
53. Sulzer P, Hartungen E, Hanel G, et al. A proton transfer reaction-quadrupole interface time-of-flight mass spectrometer (PTR-QiTOF): high speed due to extreme sensitivity. *Int J Mass Spectrom*. 2014;368:1-5.
54. Beauchamp J, Herbig J, Dunkl J, Singer W, Hansel A. On the performance of proton-transfer-reaction mass spectrometry for breath-relevant gas matrices. *Meas Sci Technol*. 2013;24(12):125003.
55. Wich T, Lüke W, Büker K, et al. Carbon2Chem®—technical center in Duisburg. *Chem Ing Tech*. 2018;90(10):1369-1374.
56. Vautz W, Schmäh M. HovaCAL®—a generator for multi-component humid calibration gases. *Int J Ion Mobil Spectrom*. 2009;12(4):139-147.
57. Koss AR, Sekimoto K, Gilman JB, et al. Non-methane organic gas emissions from biomass burning: identification, quantification, and emission factors from PTR-ToF during the FIREX 2016 laboratory experiment. *Atmos Chem Phys*. 2018;18(5):3299-3319.
58. Stockwell CE, Veres PR, Williams J, Yokelson RJ. Characterization of biomass burning emissions from cooking fires, peat, crop residue, and other fuels with high-resolution proton-transfer-reaction time-of-flight mass spectrometry. *Atmos Chem Phys*. 2015;15(2):845-865.
59. Morscheiser J, Thönnessen L, Friedrich B. Sulphur control in nickel-based superalloy production. *Proceedings—European Metallurgical Conference, EMC 2011*. 2011;4:1197-1212.
60. Sidorov VV, Min PG, Kablov DE. Desulfurization of single-crystal nickel superalloys with vacuum melting. *Metallurgist*. 2017;61(5–6):400-405.
61. Sun Q, Cheng H, Mei X, et al. Efficient synchronous extraction of nickel, copper, and cobalt from low-nickel matte by sulfation roasting–water leaching process. *Sci Rep*. 2020;10(1):9916.
62. Christien F. Role of impurity sulphur in the ductility trough of austenitic iron-nickel alloys. *Materials*. 2020;13(3):539.
63. Chehade H, Yang YD, Wu P, Barati M, McLean A. Removal of phosphorus, sulphur, and arsenic from ferronickel and nickel alloy. In: Marquis F, ed. *Proceedings of the 8th Pacific Rim International Congress on Advanced Materials and Processing*. Cham; 2016:725-733.
64. Knighton WB, Fortner EC, Midey AJ, et al. HCN detection with a proton transfer reaction mass spectrometer. *Int J Mass Spectrom*. 2009;283(1–3):112-121.
65. Dunne E, Galbally IE, Lawson S, Patti A. Interference in the PTR-MS measurement of acetonitrile at *m/z* 42 in polluted urban air—a study using switchable reagent ion PTR-MS. *Int J Mass Spectrom*. 2012;319–320:40-47.
66. Gueneron M, Erickson MH, VanderSchelden GS, Jobson BT. PTR-MS fragmentation patterns of gasoline hydrocarbons. *Int J Mass Spectrom*. 2015;379:97-109.
67. Schwarz K, Filipiak W, Amann A. Determining concentration patterns of volatile compounds in exhaled breath by PTR-MS. *J Breath Res*. 2009;3(2):027002.
68. Baasandorj M, Millet DB, Hu L, Mitroo D, Williams BJ. Measuring acetic and formic acid by proton-transfer-reaction mass spectrometry: sensitivity, humidity dependence, and quantifying interferences. *Atmos Meas Tech*. 2015;8(3):1303-1321.
69. Feilberg A, Liu D, Adamsen AP, Hansen MJ, Jonassen KE. Odorant emissions from intensive pig production measured by online proton-transfer-reaction mass spectrometry. *Environ Sci Technol*. 2010;44(15):5894-5900.
70. Ruttink PJA, Burgers PC. The gas-phase chemistry of the formic-acid radical cation $[Hcooh]^{\cdot+}$—mechanism for exchange of the hydrogen atoms—a quantum chemical investigation. *Int J Mass Spectrom*. 1992;113(1):23-33.
71. Shuman NS, Johnson M, Stevens WR, Harding ME, Stanton JF, Baer T. Tunneling in a simple bond scission: the surprising Barrier in the H loss from $HCOOH^+$. *J Phys Chem A*. 2010;114(37):10016-10023.

72. Ŝpaněl P, Smith D. SIFT studies of the reactions of H_3O^+, NO^+ and O_2^+ with a series of volatile carboxylic acids and esters. *Int J Mass Spectrom Ion Processes*. 1998;172(1–2):137-147.
73. Jobson BT, Alexander ML, Maupin GD, Muntean GG. On-line analysis of organic compounds in diesel exhaust using a proton transfer reaction mass spectrometer (PTR-MS). *Int J Mass Spectrom*. 2005;245(1–3):78-89.
74. Klein F, Platt SM, Farren NJ, et al. Characterization of gas-phase organics using proton transfer reaction time-of-flight mass spectrometry: cooking emissions. *Environ Sci Technol*. 2016;50(3):1243-1250.
75. Sarkar C, Sinha V, Kumar V, et al. Overview of VOC emissions and chemistry from PTR-TOF-MS measurements during the SusKat-ABC campaign: high acetaldehyde, isoprene and isocyanic acid in wintertime air of the Kathmandu Valley. *Atmos Chem Phys*. 2016;16(6):3979-4003.
76. Wright JS, Ingold KU. Understanding trends in C-H, N-H, and O-H bond dissociation enthalpies. *J Chem Educ*. 2000;77(8):1062-1064.
77. Kaur D, Kaur RP. Evaluation of N-H bond dissociation energies in some amides using ab initio and density functional methods. *J Mol Struc-Theochem*. 2005;757(1–3):53-59.
78. Warneke C, van der Veen C, Luxembourg S, de Gouw JA, Kok A. Measurements of benzene and toluene in ambient air using proton-transfer-reaction mass spectrometry: calibration, humidity dependence, and field intercomparison. *Int J Mass Spectrom*. 2001;207(3):167-182.
79. Tani A, Hayward S, Hewitt CN. Measurement of monoterpenes and related compounds by proton transfer reaction-mass spectrometry (PTR-MS). *Int J Mass Spectrom*. 2003;223–224:561-578.
80. de Gouw J, Warneke C, Karl T, Eerdekens G, van der Veen C, Fall R. Sensitivity and specificity of atmospheric trace gas detection by proton-transfer-reaction mass spectrometry. *Int. J. Mass Spectrom*. 2003;223–224:365-382.
81. Sinha V, Custer TG, Kluepfel T, Williams J. The effect of relative humidity on the detection of pyrrole by PTR-MS for OH reactivity measurements. *Int J Mass Spectrom*. 2009;282(3):108-111.
82. Acton WJ, Lanza M, Agarwal B, et al. Headspace analysis of new psychoactive substances using a selective reagent ionisation-time of flight-mass spectrometer. *Int J Mass Spectrom*. 2014;360:28-38.
83. Materic D, Peacock M, Kent M, et al. Characterisation of the semi-volatile component of dissolved organic matter by thermal desorption–proton transfer reaction–mass spectrometry. *Sci Rep*. 2017;7(1):15936.
84. Petrie S, Bettens RPA, Freeman CG, Mcewan MJ. Ion-molecule chemistry of $H_nC_3O^+$, $C_3O_2^+$, and C_3O^+. *J Phys Chem*. 1993;97(51):13673-13676.
85. Williams J, Pöschl U, Crutzen PJ, et al. An atmospheric chemistry interpretation of mass scans from a PTR-MS flown over Surinam. *J Atmos Chem*. 2001;38(2):133-166.
86. Muller M, Mikoviny T, Feil S, et al. A compact PTR-ToF-MS instrument for airborne measurements of volatile organic compounds at high spatiotemporal resolution. *Atmos Meas Tech*. 2014;7(11):3763-3772.
87. Papurello D, Tomasi L, Silvestri S, et al. Biogas trace compound removal with ashes using proton transfer reaction time-of-flight mass spectrometry as innovative detection tool. *Fuel Process Technol*. 2016;145:62-75.
88. Jordan A, Haidacher S, Hanel G, et al. A high resolution and high sensitivity proton-transfer-reaction time-of-flight mass spectrometer (PTR-TOF-MS). *Int J Mass Spectrom*. 2009;286(2–3):122-128.
89. Smith D, Španěl P. Selected ion flow tube mass spectrometry (SIFT-MS) for on-line trace gas analysis. *Mass Spectrom Rev*. 2005;24(5):661-700.
90. Warneke C, Holzinger R, Hansel A, et al. Isoprene and its oxidation products methyl vinyl ketone, methacrolein, and isoprene related peroxides measured online over the tropical rain forest of Surinam in March 1998. *J Atmos Chem*. 2001;38(2):167-185.
91. Silvis ICJ, Luning PA, Klose N, Jansen M, van Ruth SM. Similarities and differences of the volatile profiles of six spices explored by proton transfer reaction mass spectrometry. *Food Chem*. 2019;271:318-327.
92. Tanimoto H, Aoki N, Inomata S, Hirokawa J, Sadanaga Y. Development of a PTR-TOFMS instrument for real-time measurements of volatile organic compounds in air. *Int J Mass Spectrom*. 2007;263(1):1-11.
93. Španěl P, Smith D. Reactions of hydrated hydronium ions and hydrated hydroxide ions, with some hydrocarbons and oxygen-bearing organic-molecules. *J Phys Chem*. 1995;99(42):15551-15556.
94. Fiches G, Deleris I, Saint-Eve A, Brunerie P, Souchon I. Modifying PTR-MS operating conditions for quantitative headspace analysis of hydro-alcoholic beverages. 2. Brandy characterization and discrimination by PTR-MS. *Int J Mass Spectrom*. 2014;360(1):15-23.
95. Karl T. Use of proton-transfer-reaction mass spectrometry to characterize volatile organic compound sources at the La Porte super site during the Texas Air Quality Study 2000. *J Geophys Res*. 2003;108(D16):4508.
96. Aprea E, Biasioli F, Märk TD, Gasperi F. PTR-MS study of esters in water and water/ethanol solutions: fragmentation patterns and partition coefficients. *Int J Mass Spectrom*. 2007;262(1–2):114-121.
97. Kaser L, Karl T, Schnitzhofer R, et al. Comparison of different real time VOC measurement techniques in a ponderosa pine forest. *Atmos Chem Phys*. 2013;13(5):2893-2906.
98. Schuhfried E, Probst M, Limtrakul J, et al. Sulfides: chemical ionization induced fragmentation studied with proton transfer reaction-mass spectrometry and density functional calculations. *J Mass Spectrom*. 2013;48(3):367-378.
99. Španěl P, Zabka J, Zymak I, Smith D. Selected ion flow tube study of the reactions of H_3O^+ and NO^+ with a series of primary alcohols in the presence of water vapour in support of selected ion flow tube mass spectrometry. *Rapid Commun Mass Spectrom*. 2017;31(5):437-446.
100. Beauchamp J, Herbig J. Proton-transfer-reaction time-of-flight mass spectrometry (PTR-TOFMS) for aroma compound detection in real-time: technology, developments, and applications. *Chemical Sensory Informatics of Food: Measurement, Analysis, Integration*. 2015;1191:235-251.
101. Materic D, Lanza M, Sulzer P, et al. Monoterpene separation by coupling proton transfer reaction time-of-flight mass spectrometry with fastGC. *Anal Bioanal Chem*. 2015;407(25):7757-7763.
102. Misztal PK, Heal MR, Nemitz E, Cape JN. Development of PTR-MS selectivity for structural isomers: monoterpenes as a case study. *Int J Mass Spectrom*. 2012;310:10-19.
103. Brilli F, Ruuskanen TM, Schnitzhofer R, et al. Detection of plant volatiles after leaf wounding and darkening by proton transfer reaction "time-of-flight" mass spectrometry (PTR-TOF). *PLoS One*. 2011;6(5):e20419.
104. Nenadis N, Heenan S, Tsimidou MZ, Van Ruth S. Applicability of PTR-MS in the quality control of saffron. *Food Chem*. 2016;196:961-967.
105. Bruhova Michalcikova R, Dryahina K, Smith D, Španěl P. Volatile compounds released by Nalophan; implications for selected ion flow tube mass spectrometry and other chemical ionisation mass spectrometry analytical methods. *Rapid Commun Mass Spectrom*. 2020;34(5):e8602.
106. Steele DA, Short RD, Brown P, Mayhew CA. On the use of SIFT-MS and PTR-MS experiments to explore reaction mechanisms in plasmas of volatile organics: siloxanes. *Plasma Processes Polym*. 2011;8(4):287-294.

107. Stone JA, Wojtyniak ACM, Wytenburg W. The condensation of trimethylsilylium with water and the proton affinity of trimethylsilanol. *Can J Chem*. 1986;64(3):575-576.
108. Langford V, Gray J, Maclagan R, McEwan M. Detection of siloxanes in landfill gas and biogas using SIFT-MS. *Curr Anal Chem*. 2013;9(4):558-564.
109. Španěl P, Smith D. Selected ion flow tube studies of the reactions of H_3O^+, NO^+, and O_2^+ with several aromatic and aliphatic hydrocarbons. *Int J Mass Spectrom*. 1998;181(1–3):1-10.
110. Yuan B, Koss AR, Warneke C, Coggon M, Sekimoto K, de Gouw JA. Proton-transfer-reaction mass spectrometry: applications in atmospheric sciences. *Chem Rev*. 2017;117(21):13187-13229.
111. Yokelson RJ, Burling IR, Gilman JB, et al. Coupling field and laboratory measurements to estimate the emission factors of identified and unidentified trace gases for prescribed fires. *Atmos Chem Phys*. 2013;13(1):89-116.
112. Manoukian A, Quivet E, Temime-Roussel B, Nicolas M, Maupetit F, Wortham H. Emission characteristics of air pollutants from incense and candle burning in indoor atmospheres. *Environ Sci Pollut Res Int*. 2013;20(7):4659-4670.
113. Urban W, Lohmann H, Salazar Gomez JI. Catalytically upgraded landfill gas as a cost-effective alternative for fuel cells. *J Power Sources*. 2009;193(1):359-366.
114. Ajhar M, Wens B, Stollenwerk KH, Spalding G, Yuce S, Melin T. Suitability of Tedlar gas sampling bags for siloxane quantification in landfill gas. *Talanta*. 2010;82(1):92-98.
115. Ghidotti M, Fabbri D, Torri C. Determination of linear and cyclic volatile methyl siloxanes in biogas and biomethane by solid-phase microextraction and gas chromatography-mass spectrometry. *Talanta*. 2019;195:258-264.
116. Jiao CQ, DeJoseph CA, Garscadden A. Ion chemistries in hexamethyldisiloxane. *J Vac Sci Technol A*. 2005;23(5):1295-1304.
117. Tang XC, Misztal PK, Nazaroff WW, Goldstein AH. Siloxanes are the most abundant volatile organic compound emitted from engineering students in a classroom. *Environ Sci Technol Lett*. 2015;2(11):303-307.

SUPPORTING INFORMATION

Additional supporting information may be found online in the Supporting Information section at the end of this article.

How to cite this article: Salazar Gómez JI, Sojka M, Klucken C, Schlögl R, Ruland H. Determination of trace compounds and artifacts in nitrogen background measurements by proton transfer reaction time-of-flight mass spectrometry under dry and humid conditions. *J Mass Spectrom*. 2021;56(8):e4777. https://doi.org/10.1002/jms.4777